Author Manuscript

Author Manuscript

Author Manuscript

Author Manuscript

HHS Public Access

Author manuscript

Neuroimage. Author manuscript; available in PMC 2024 March 18.

Published in final edited form as:

Neuroimage. 2023 June ; 273: 120068. doi:10.1016/j.neuroimage.2023.120068.

Multimodal comparisons of QSM and PET in neurodegeneration and aging

Petrice M. Cogswell[a,*], **Audrey P. Fan**[b]

[a]Department of Radiology, Mayo Clinic, 200 First St SW, Rochester, MN 55905, USA

[b]Department of Biomedical Engineering and Department of Neurology, University of California, Davis, 1590 Drew Avenue, Davis, CA 95618, USA

Abstract

Quantitative susceptibility mapping (QSM) has been used to study susceptibility changes that may occur based on tissue composition and mineral deposition. Iron is a primary contributor to changes in magnetic susceptibility and of particular interest in applications of QSM to neurodegeneration and aging. Iron can contribute to neurodegeneration through inflammatory processes and via interaction with aggregation of disease-related proteins. To better understand the local susceptibility changes observed on QSM, its signal has been studied in association with other imaging metrics such as positron emission tomography (PET). The associations of QSM and PET may provide insight into the pathophysiology of disease processes, such as the role of iron in aging and neurodegeneration, and help to determine the diagnostic utility of QSM as an indirect indicator of disease processes typically evaluated with PET. In this review we discuss the proposed mechanisms and summarize prior studies of the associations of QSM and amyloid PET, tau PET, TSPO PET, FDG-PET, 15O-PET, and F-DOPA PET in evaluation of neurologic diseases with a focus on aging and neurodegeneration.

Keywords

Quantitative susceptibility mapping (QSM); Amyloid PET; Tau PET; TSPO PET; F-dopa PET; Neurodegenerative disease

1. Introduction

Aging and neurologic diseases may cause a change in tissue composition, such as mineral or protein deposition or change in myelin or lipid content (Collingwood et al., 2005; Deibel et al., 1996; Lassmann and van Horssen, 2011; Popescu et al., 2013; Sofic et al., 1988). Detection and monitoring of such pathologic changes is a broad focus of research across

This is an open access article under the CC BY-NC-ND license (http://creativecommons.org/licenses/by-nc-nd/4.0/)

*Corresponding author. Cogswell.petrice@mayo.edu (P.M. Cogswell).

Declaration of Competing Interest

Authors declare that they have no conflict of interest.

Credit authorship contribution statement

Petrice M. Cogswell: Conceptualization, Investigation, Writing – original draft. **Audrey P. Fan:** Conceptualization, Investigation, Writing – original draft.

Author Manuscript Author Manuscript Author Manuscript Author Manuscript

imaging modalities. One of the more recently developed methods to non-invasively probe brain tissue composition with MRI is quantitative susceptibility mapping (QSM) (Li et al., 2011; Sood et al., 2017). QSM is an MRI technique that allows quantification of local tissue magnetic susceptibility via complex post-processing (phase unwrapping, masking, background field removal, and inversion) of a multi-echo gradient-recalled echo (GRE) acquisition (de Rochefort et al., 2008; Haacke et al., 2015; Li et al., 2011; Liu et al., 2015; Shmueli et al., 2009). The output is a map of magnetic susceptibilities with negative values indicating diamagnetic tissue properties and positive values indicating paramagnetic properties relative to a selected tissue reference. Compared to other susceptibility sensitive sequences, such as T2*-weighting imaging, QSM is quantitative, reflects local vs. nonlocal tissue properties, is more sensitive to susceptibility effects, and is less dependent on imaging parameters and object orientation. In the brain, QSM has been used to study susceptibility changes that may occur based on the content of iron, calcium, myelin or lipids in a wide range of neurologic diseases (Ravanfar et al., 2021; Uchida et al., 2022; Wang and Liu, 2015).

Iron is of particular interest in applications of QSM to neurodegeneration and aging. Independent of a specific neurodegenerative disease, iron can contribute to cell death and neuronal loss through inflammatory processes, including induction of oxidative damage and production of reactive oxygen species, as well as iron related cell death or “ferroptosis” (Dixon et al., 2012; Lane et al., 2018; Li et al., 2020). Iron has also been shown to contribute to neurodegeneration via interaction with aggregation of disease-related proteins such as amyloid plaques, tau neurofibrillary tangles, and alpha-synuclein (Meadowcroft et al., 2009; Ndayisaba et al., 2019; Smith et al., 1997).

To better understand the local susceptibility changes observed on QSM, its signal has been studied in association with other imaging metrics such as positron emission tomography (PET). In PET, the distribution of an intravenously administered radiotracer is captured, and, depending on the nature of the radiotracer, may target deposition of specific proteins or neurochemical processes (Hooker and Carson, 2019). The associations of QSM and PET may provide insight into the pathophysiology of disease processes, such as the role of iron in the aging and neurodegeneration (Deistung et al., 2013; Ravanfar et al., 2021; Vinayagamani et al., 2021; Wang et al., 2017), and help to determine the diagnostic utility of QSM as an indirect indicator of disease processes typically evaluated with PET, such as amyloid load (Acosta-Cabronero et al., 2016; Bergen et al., 2016; Bilgic et al., 2012; Cogswell et al., 2021; Fazlollahi et al., 2017b; Gong et al., 2019; Kim et al., 2017; Ravanfar et al., 2021; Tiepolt et al., 2018, 2021; van Bergen et al., 2018). Furthermore, PET tracers can directly assess the presence of microglial cells that drive the neuroinflammatory response to pathological deposits and iron accumulation, as well as its downstream effects on brain glucose metabolism and synaptic function. Associating these PET signals with QSM would also augment understanding of the complex, spatiotemporal evolution of neuroinflammation with iron, and its link to brain functional changes in aging and neurodegeneration.

In this review we discuss the proposed mechanisms and summarize prior studies of the associations of QSM and PET for various PET tracers in evaluation of neurologic diseases with a focus of those related to aging and neurodegeneration. We describe the brain regions

Author Manuscript Author Manuscript Author Manuscript Author Manuscript

in which these imaging metrics have been compared for specific disorders and highlight how the QSM signal complements information from relevant PET tracers. We also include discussion of studies using T2 * /R2* as an indicator of iron deposition in diseases in which limited QSM data exists.

2. Mechanism-based review of QSM-PET comparisons

2.1. Amyloid PET

Alzheimer's disease (AD) is characterized by accumulation of amyloid plaques and tau tangles (Jack et al., 2018). In vivo assessment of amyloid pathology may be achieved with amyloid PET, CSF, and more recently plasma, with PET being the most direct measure of cumulative amyloid deposition (Janelidze et al., 2021; Johnson et al., 2013; Schindler et al., 2019; Shaw et al., 2018). Amyloid PET is widely used in research and clinical trials for assessment of Alzheimer's pathologic change and provides regional brain information about the presence of amyloid (Cummings et al., 2022; Swanson et al., 2021).

Amyloid PET radiotracers targeting Aβ in amyloid plaques include Pittsburgh compound B (11C-PiB) (Klunk et al., 2004), 18F-florbetapir (Lister-James et al., 2011), 18F- florbetaben, and 18F-flumetamol. Although some studies have found regional amyloid PET changes to provide biologically-relevant information about disease stage (Collij et al., 2022; Grothe et al., 2017; Jelistratova et al., 2020), amyloid PET is most commonly assessed via magnitude of a global meta-ROI (Mintun et al., 2006).

The relationship of QSM and amyloid PET is of high interest given the coexistence of iron with amyloid plaques. Although multiple studies have demonstrated that iron accumulates near amyloid plaques and facilitates plaque formation (Hautot et al., 2003; Plascencia-Villa et al., 2016; Smith et al., 1997; Telling et al., 2017), the mechanism of this association is not well understood. In histochemical and x-ray microscopy studies, iron has been shown to exist in a complex with and/or coexist with amyloid plaques, trigger ferroptosis, and promote oxidative stress (Derry and Kent, 2017; Everett et al., 2014; Plascencia-Villa et al., 2016; Smith et al., 1997; Telling et al., 2017). In ex vivo studies and in vivo mouse models, iron has been used as the basis of contrast for identification of amyloid plaques (Jack et al., 2004; Meadowcroft et al., 2009). Based on the co-occurrence of iron and amyloid plaque in molecular studies, animal models, and ex vivo human studies, it has been proposed that QSM may be used to identify iron and infer the presence of amyloid in vivo.

In vivo studies of the association of amyloid PET and susceptibility have shown a positive association in the basal ganglia (Cogswell et al., 2021; Tiepolt et al., 2018; van Bergen et al., 2018), where there are relatively higher levels of age-related iron deposition compared to elsewhere in the brain (Bilgic et al., 2012; Li et al., 2014). However, in the cerebral cortex, where we are interested in detecting AD-related amyloid accumulation, the associations of amyloid PET and QSM have been variable. While some studies have shown a positive association of amyloid PET SUVR and susceptibility in the frontal and temporal cortex (Ayton et al., 2017; van Bergen et al., 2018), others have shown no or very weak negative associations in those regions (Chen et al., 2021b; Cogswell et al., 2021; Tiepolt et al., 2018). Higher susceptibility and post-mortem iron levels have also been found to be associated with

Author Manuscript Author Manuscript Author Manuscript Author Manuscript

greater cognitive decline, however, only in amyloid positive individuals with mild cognitive impairment (Ayton et al., 2019, 2017).

While there are differences in populations and analysis techniques that may account for some of the differences in prior amyloid PET-QSM studies, the lack of an expected positive association of amyloid PET and susceptibility may be related to local competing paramagnetic and diamagnetic effects in the cortex. Ex vivo studies have shown that amyloid aggregates have diamagnetic properties that may oppose paramagnetic changes of iron (Gong et al., 2019). With new QSM algorithms designed to separate paramagnetic and diamagnetic components (Chen et al., 2021a; Shin et al., 2021), individual effects of iron and amyloid may be better evaluated, and thereby achieve better associations with amyloid PET. To date, in vivo applications of these techniques have been limited to few studies in multiple sclerosis (Dimov et al., 2022; Emmerich et al., 2021). Please refer to a complimentary review article in this special issue of Neuroimage for additional commentary on future direction of QSM in the study of AD.

Amyloid may also be deposited in the vessel wall of arteries and arterioles and result in cerebral amyloid angiopathy (CAA), which increases the risk of micro and macro-hemorrhages (Greenberg et al., 2020). The amyloid deposition in CAA has been found to be associated with an increase in cortical amyloid PET SUVR, particularly in the occipital cortex, where there is a predilection for CAA pathology (Greenberg et al., 2008; Johnson et al., 2007). However, the coexistence of parenchymal amyloid deposits of AD and vascular amyloid of CAA as well as the relatively high QSM signal of heme-related iron in the vessels and hemorrhages make study of vascular amyloid-related PET signal challenging, especially with typical PET spatial resolution of 2–5 mm. Therefore, studies of amyloid PET in CAA have been limited to participants without dementia and applied for detection of early CAA and evaluation of patients with possible CAA by the Boston Criteria (Charidimou et al., 2017; Greenberg and Charidimou, 2018). QSM in CAA has focused on the detection of cerebral microbleeds (Rotta et al., 2021). Direct comparisons of QSM and PET in CAA are lacking and would similarly be challenging due to the challenges in distinguishing vascular and parenchymal amyloid deposits.

2.2. Tau PET

Tau, the other major pathologic protein of AD, is deposited in the brain as neurofibrillary tangles and is strongly associated with neurodegeneration and cognitive decline (Braak and Braak, 1991; Hyman et al., 2012; Johnson et al., 2016; Ossenkoppele et al., 2016). Like amyloid, tau load may be assessed in vivo via PET and CSF, and plasma biomarkers are emerging (Jack et al., 2018; Janelidze et al., 2020; Mielke et al., 2021, 2018). First-generation tau PET ligands include [18F]THK5317, [18F] THK5351, [18F]AV1451 (flortaucipir), and [11C]PBB3; and second-generation ligands, developed to reduce off-target binding, include [18F]MK-6240, [18F]RO-948 [18F]PI-2620, [18F]GTP1, [18F] PM-PBB3, and [18F]JNJ64349311 (Leuzy et al., 2019; Lois et al., 2019). In the study of AD, tau PET has been evaluated based on the magnitude of signal in the temporal meta-ROI (Jack et al., 2017) and topographic distribution in the cortex, which may provide information about disease subtype and stage (Ossenkoppele et al., 2016; Therriault et al., 2022; Vogel

Author Manuscript Author Manuscript Author Manuscript Author Manuscript

et al., 2021). As with amyloid plaques, iron has been proposed to exist in complex with tau aggregates and contribute to oxidative stress (Derry and Kent, 2017).

Studies of the associations of tau PET and QSM in the context of aging and AD have evaluated the cortex and deep gray structures with voxel-wise and ROI-based approaches. In the basal ganglia, a strong association has been found between age-related iron accumulation and tau PET SUVR (18F-AV-1451) (Choi et al., 2018; Cogswell et al., 2021) (Fig. 1). The tau PET signal in this region is thought to be related to off-target binding of the tau ligand, secondary to monoamine oxidate (MAO) and/or iron deposition in the setting of inflammation (Baker et al., 2019; Harada et al., 2018; Lemoine et al., 2018).

In the cortex, susceptibility and tau PET SUVR (18F-RO-948) have been found to be associated in the temporal lobe (Spotorno et al., 2020). The mechanism of this association may be iron associated with AD-related tau aggregation. This hypothesis was supported by Spotorno et al. who found cortical susceptibility mediated the effect of tau on neurodegeneration in amyloid positive individuals. Alternatively, other processes such as iron deposition with inflammation and off target tau binding may occur in the cortex as in the basal ganglia. Either of these processes may result in neurodegeneration and therefore the association of iron and neurodegeneration (Cogswell et al., 2021; Spotorno et al., 2020). Variability in results of studies evaluating associations of QSM and tau PET may in part be related to the tau PET tracer and degree of off-target binding. Additionally, although a positive association of tau PET and paramagnetic susceptibility has been found in some studies, an ex vivo study detected diamagnetic signal association with tau protein in solution (Gong et al., 2019). As with amyloid, tau aggregation in the cortex, may therefore cause QSM signal that opposes that of colocalized iron in AD.

Other tauopathies, such as progressive supranuclear palsy (PSP), have been studied with QSM and tau PET (Leuzy et al., 2019; Lois et al., 2019; Ravanfar et al., 2021; Uchida et al., 2022), but studies correlating QSM and PET are limited. For example, QSM studies have shown increased susceptibility in the putamen, globus pallidus, red nucleus and substantia nigra in patients with PSP compared to controls (Ravanfar et al., 2021; Sjöström et al., 2017). Elevated tau PET signal has been found in patients with PSP compared to those with AD and cognitively unimpaired controls in similar basal ganglia and midbrain regions as those of increased magnetic susceptibility (Brendel et al., 2020; Whitwell et al., 2017). A recent study directly compared QSM susceptibility and tau PET SUVR in PSP vs. controls and found that susceptibility and SUVR were well-correlated and higher in PSP that controls in the pallidum, red nucleus and cerebellar dentate (Satoh et al., 2023).

2.3. TSPO PET

Neuroinflammation is a complex process that in pathological states correlates with iron deposition and ultimately neurodegeneration through several mechanisms, thus requiring multi-variate observations to understand its spatiotemporal patterns. An inflammatory cascade that is common across numerous neurodegenerative disorders happens in response to abnormal protein aggregates, ranging from amyloid in AD; tau in AD and progressive supranuclear palsy; alpha-synuclein in Parkinson’s disease; and TDP-43 (TAR DNA-binding protein 43) in frontotemporal dementia (Nnah and Wessling-Resnick, 2018). The misfolding

Author Manuscript Author Manuscript Author Manuscript Author Manuscript

and accumulation of these toxic proteins activates microglial cells, which form the primary immune response of the central nervous system and sequester the excess iron and ferritin that occurs in oxidative stress (Nnah and Wessling-Resnick, 2018). In this way, the detection of iron on T2*-weighted or QSM signal is an indirect measure of inflammation-related iron metabolism and the presence of microglia.

Histologically, T2* MRI signal has been directly associated with iron and amyloid stains in human AD tissue samples from the entorhinal cortex (Meadowcroft et al., 2009); while other studies have shown focal T2* hypo-intensities in micro-infarcts that are best colocalized to microglia and iron stains in the subiculum (a subfield of the hippocampus), even in the absence of amyloid and tau pathology (Zeineh et al., 2015). These findings suggest that both protein deposition-related and incidental micro-infarcts lead to inflammatory responses and concomitant iron deposition, and that multi-modal correlative studies in vivo will be key to investigate different underlying pathophysiology. Overall, the coordination between microglial activity and iron uptake is complicated, such that balance between beneficial pro-inflammatory processes and damage from chronic neuroinflammation likely depend on the disease stage and brain regions for a given neurodegenerative disorder.

In vivo PET imaging of microglial activation (i.e., during neuroinflammation) is to date primarily achieved by targeting the 18-kDa translocator protein (TSPO) in the outer membrane of the mitochondria. Because there is low baseline expression of TSPO in the central nervous system, increases in brain TSPO-PET signal are sensitive to upregulation in activated microglia and can be combined with information from separate amyloid- and tau-PET studies in the same patients. The evolution of TSPO-PET radioligands has been well-described (Alam et al., 2017; Gouilly et al., 2022; Lagarde et al., 2018); and both first-([11C]PK11195) and second-generation (e.g., [11C]-PBR28, [18F]-DPA714) tracers have been correlated with amyloid and tau PET in mild cognitive impairment (MCI) and AD. These associations were performed voxelwise and across larger cortical regions, revealing positive relationships between amyloid PET uptake in broad frontal, parietal, and lateral temporal areas (MCI and AD) (Chandra et al., 2019; Parbo et al., 2018); as well as in smaller regions as the hippocampus (MCI) (Knezevic and Mizrahi, 2018). Similar clusters of positive association between tau- and TSPO-PET signals have been observed in association cortices, in particular in the frontal and temporal cortex of MCI patients and the parietal cortex of AD patients (Dani et al., 2018). While these correlative studies link the presence of pathological protein aggregates to neuroinflammatory processes, there is a future need to similarly correlate cortical TSPO-PET signal to QSM and/or T2* signal indicating iron. PET/MRI comparisons are underway in chronic fatigue syndrome, where trends of elevated QSM and R2* relaxation (indicating high iron levels) were observed alongside higher TSPO PET signal ([11C] DPA-713) in putamen regions of patients relative to healthy controls (Carlson et al., 2020) .

TSPO and [62Cu]diacetyl-bis(N4-methylthiosemicarbazone) (62Cu-ATSM) PET have also been applied to Amyotrophic lateral sclerosis (ALS), a disorder of upper and lower motor neuron degeneration, as indicators of neuroinflammation and oxidative stress, respectively. Studies have shown greater activity in the motor cortex, which was associated with higher disease severity (Chew and Atassi, 2019; Ikawa et al., 2015). QSM studies have similarly

Author Manuscript Author Manuscript Author Manuscript Author Manuscript

shown increased susceptibility of the motor cortex in patients with ALS (Acosta-Cabronero et al., 2018; Schweitzer et al., 2015), which may be related to accumulation of iron-containing microglia (Kwan et al., 2012). However, there has not been a direct comparison of TSPO or 62Cu-ATSM PET and susceptibility in ALS patients to date.

In addition to inflammatory responses to protein aggregates and neurodegeneration, the relationship between microglial activity and iron deposition is also of high clinical value in autoimmune disorders such as multiple sclerosis (MS). Chronically active MS lesions show a hyperintense (high susceptibility) rim of iron-laden microglia and macrophages, indicative of persistent disease-related inflammation that leads to greater tissue damage. Using simultaneous PET/MRI scans with [11C]-PK11195 TSPO tracer and QSM, Kaunzner et al. demonstrated that these lesions with high susceptibility also had higher TSPO signal, validating the colocalization of activated microglia with iron accumulation at the lesion border (Kaunzner et al., 2019). Mechanistically, this association could reflect intracellular iron within active microglia that respond to myelin and oligodendrocyte debris during demyelination in MS; or that iron is released by oligodendrocytes in white matter near MS lesions as a downstream effect of microglial activation. Both lesion-specific and broader analyses of TSPO-PET and QSM/T2* signal correlations across the cortex or cortical layers offer meaningful insight into the heterogeneity of MS lesions (Fig. 2) (Herranz et al., 2020). The comparison would enable QSM signal to better differentiate lesions based on inflammatory status and chronicity, and offer a non-invasive MRI method to understand the impact of these lesions on MS progression.

Overall, the limitations of studying neuroinflammation with TSPO-PET alone include limited binding affinity in individuals with certain genetic polymorphisms of the TSPO protein (Owen et al., 2012); lack of discrimination between microglial activation states; and sensitivity of the PET signal to reactive astrocytes that play a different role than microglia (Lavisse et al., 2012). Newer TSPO tracers such as ER176 may address some of the limitations with binding, as ER176 is shown to have higher binding potential and less measurement variability (e.g., of distribution volume metrics) when compared head-to-head with earlier TSPO tracers (Zanotti-Fregonara et al., 2019). ER176 is also the only TSPO tracer that is suitable for use in low-affinity binders (Fujita et al., 2017), and due to its high binding, likely requires smaller subject sample size for similar statistical power in study design (Zanotti-Fregonara et al., 2019). Beyond TSPO, new radioligands have targeted monoamine oxidase-B (MAO-B) and imidazoline2 (I2BS) binding sites that are highly expressed in reactive astrogliosis. Although these tracers also face limitations in off-target binding, MAO-B and I2BS PET provide specificity to reactive astrocytes that lead to distinct pro-inflammatory cascades in parallel with microglial activation (Kwon and Koh, 2020), each pathway contributing to neurodegeneration. The chronicity and phases of these complex mechanisms is still under investigation, for instance in identifying when classically activated microglia induce certain subtypes of astrocytes (Liddelow et al., 2017), and the transition from beneficial clearance of toxic proteins versus harmful (excitotoxic) neuroinflammation (Kaur et al., 2019).

In the future, direct in vivo correlations of neuroinflammation PET with QSM-based iron deposition will enable improved: (a) monitoring of inflammation-related iron

Author Manuscript Author Manuscript Author Manuscript Author Manuscript

accumulation at early disease stages and its causal progression; (b) multi-modal understanding of transition between beneficial versus detrimental neuroinflammatory phases at different disease stages; and (c) knowledge of the extent to which QSM signal as a sensitive MRI-only marker for iron dysregulation is attributable to abnormal microglial activity. This information offers powerful multi-modal biomarkers for early detection of neuroinflammation with its pathological underpinnings and monitoring anti-inflammation response to disease-modifying therapies.

2.4. FDG-PET

[18F]-fluorodeoxyglucose (FDG) is the most common PET radiotracer and assesses glucose metabolism as a surrogate marker for neuronal function and integrity. Distinct spatial patterns of reduced glucose metabolism on FDG-PET are clinically used to differentiate Alzheimer's disease from other dementias (Mosconi et al., 2008), including frontotemporal dementia and dementia with Lewy Bodies (Minoshima et al., 2021). FDG-PET has also been proposed for differentiation of PSP subtypes and PD (Zhao et al., 2020). In Alzheimer's disease, the longitudinal decrease of FDG-PET signal, indicating deficit in the cerebral metabolic rate of glucose, is prominent in the hippocampus, parietotemporal, and posterior cingulate cortices (Mosconi et al., 2009). The FDG-PET signal declines in a manner that tracks with cognitive status and complements the predictive information from other biomarkers such as amyloid (Chételat et al., 2020).

In a meta-analysis, Rao et al. reported colocalization of high brain iron (high QSM) and glucose hypometabolism (low FDG-PET signal) in the frontal, parietal, and temporal cortices as well as the thalamus of both Alzheimer's and Parkinson's patients across studies (Rao et al., 2022). The studies included in this analysis either evaluated brain iron accumulation or low glucose metabolism using imaging, but typically not both. Disease-specific regional colocalization of the two biomarkers (such as in the hippocampus of Alzheimer's disease) suggest iron-mediated brain dysfunction in focal areas known for pathological protein deposition; but also broader network-level dysfunction, such as the parietal lobe in Parkinson's disease, associated with movement impairment. There are limited studies in elderly adults that directly correlate QSM-MRI with FDG-PET; T2* signal from the subcortical nuclei did not correlate with FDG-PET in a study of a cognitively unimpaired cohort (Stankeviciute et al., 2022). More multi-modal studies are necessary to clarify specific mechanisms (i.e., QSM-PET indicating iron accumulation) that underlie reduced glucose metabolism, and to ultimately better leverage FDG-PET information as a ubiquitous tracer in clinical settings.

In contrast to Alzheimer's disease, patients with a clinical diagnosis of cerebral small vessel disease (SVD) exhibit abnormalities of brain microvessels, often with a hypertensive etiology, and present with distinct patterns of glucose hypometabolism on FDG-PET. For SVD patients, clinical diagnosis is often performed based on features such as small infarcts or white matter lesions on MRI (Vemuri et al., 2022), with FDG-PET providing visualization of brain vascular dysfunction in perturbed areas. While patients with probable AD primarily have hypometabolism in temporoparietal and frontal association areas, in patients with SVD, the FDG-PET signal shows scattered foci of hypometabolism across

Author Manuscript Author Manuscript Author Manuscript Author Manuscript

wide cerebral regions (Heiss, 2018). In addition to these broad deficits, hypometabolism was more severe in subcortical areas and primary sensorimotor cortex and less affected in association areas for SVD compared to AD.

Independently, a QSM-MRI investigation of primarily hypertensive SVD patients showed pathologically elevated iron deposition in the putamen and caudate nucleus, in a similar spatial pattern to that observed in AD patients of the same study (Moon et al., 2016). This pattern mimics non-specific iron accumulation in the basal ganglia that occurs with age, especially as controls in this study were much younger (average of 47 years) compared to SVD patients and AD groups (average of 79 years). QSM signal in SVD thus may reflect a combination of vascular damage and aging processes; and could be correlated with FDG-PET to understand the pathophysiology in affected brain regions. QSM patterns are likely different in patients with SVD caused by cerebral amyloid angiopathy, which is expected to show paramagnetic susceptibility signal both due to iron colocalized with vascular deposits of amyloid, as described above, and due to microhemorrhages that result from CAA (Charidimou et al., 2012). QSM-MRI is highly sensitive to such cortical microbleeds, even more so than T2* signal, and in combination with FDG-PET can reveal differential etiology of SVD and its impact on brain vascular function (Lee et al., 2022; Tu et al., 2022).

A major limitation of FDG-PET, however, is its lack of specificity to pathological mechanisms. Because FDG signal is linked to the local extent of brain glutamatergic activity in synapses and astrocytes (Zimmer et al., 2017), a lower FDG-PET signal is often interpreted as neuronal dysfunction and reduced brain activity in neurodegeneration. However, FDG-PET is also highly correlated with cerebral blood flow patterns (Anazodo et al., 2018; Ceccarini et al., 2020), and its quantification is influenced by blood glucose and stimulus levels. With respect to neuroinflammation, increased FDG-PET indirectly indicates the presence of activated microglia, with elevated glucose consumption via anaerobic pathways, although more sophisticated kinetic modeling approaches are necessary to isolate inflammation-related FDG-PET signal (Yang et al., 2015). Given the complexity of neuroinflammation, it is possible that QSM correlates positively with high FDG signal in the acute, early phases of the neuroinflammatory response; while QSM may correlate with lower FDG signal in later, chronic stages of the neuroinflammatory process when neural activity has declined. These considerations make it difficult to interpret specific FDG-PET and MRI correlations that may evolve with disease stage and pathology, especially in the background of high intrinsic glucose consumption in the brain. To mitigate this limitation, cross-comparisons with newer PET ligands targeting synaptic vesicle glycoprotein 2A (SV2A), a specific marker of synaptic density, have revealed regional differences in the relationship between synaptic density (SV2A-PET) and glucose metabolism (FDG-PET), thus informing the interpretation of FDG-PET as a marker of brain dysfunction. High inter-tracer correlations between synaptic density and brain metabolism were observed in medial temporal regions of elderly and Alzheimer’s patients and lower correlations in neocortical areas (Chen et al., 2021c).

Author Manuscript Author Manuscript Author Manuscript Author Manuscript

2.5. [15O]-PET

Beyond FDG PET, correlation of QSM signal with specialized [15O]-labeled PET tracers can reveal specific associations of SVD pathology with cerebral blood flow and oxygen metabolism of brain tissues. Oxygen metabolism and perfusion have been shown to decline with age (Takada et al., 1992; Yamaguchi et al., 1986) and neurodegenerative processes (Ishii et al., 1996) using the gold standard of [15O]-PET. However, in SVD patients, the opposite trend of increased oxygen extraction fraction (OEF) is observed with higher white matter hyperintensity burden (Tohgi et al., 1998; Yamaji et al., 1997) and vascular risk factors (Jiang et al., 2020). This OEF elevation may occur as a compensatory mechanism for ischemic hypoperfusion in cerebrovascular disease, including CAA; such that OEF versus cerebral blood flow / FDG-PET may show a different direction of correlation with QSM signal. To overcome the experimental challenges of [15O]-PET scans with short-lived tracers, new MRI-based methods have also leveraged the sensitivity of QSM to paramagnetic deoxyhemoglobin to assess OEF. These QSM methods measure regional OEF either intravascularly in resolvable veins (Berg et al., 2021; Fan et al., 2014), or apply a quantitative extravascular model to estimate voxelwise tissue OEF with assumptions about the blood volume (Cho et al., 2021, 2018). The novel susceptibility MRI measures of OEF are detailed in a separate review article in this special issue.

2.6. 18F-DOPA PET

18F-fluorodopa (18F-DOPA) PET allows for in vivo assessment of the integrity and function of dopaminergic neurons (Garnett et al., 1983). Specifically, 18F-DOPA targets aromatic amino acid decarboxylase (AADC), which facilitates the conversion of L-DOPA to dopamine, and is therefore an indicator of dopamine terminal activity (Loane and Politis, 2011). The primary clinical and research application of 18F-DOPA PET is assessment of loss of dopaminergic neurons in the basal ganglia in Parkinson's Disease (PD) (Morrish et al., 1996; Snow et al., 1993).

On pathology, PD is characterized by loss of dopaminergic neurons and accumulation of α-synuclein as well as iron in the substantia nigra pars compacta (SNc) (Sofic et al., 1988). As discussed in the neuroinflammation section, iron may promote α-synuclein aggregation via inflammation and oxidative stress (Hashimoto et al., 1999). Several QSM studies have shown higher susceptibility in the SN in patients with PD compared to controls, presumably reflective of iron deposition (Du et al., 2016; He et al., 2015; Murakami et al., 2015).

Limited studies exist on the association of 18F-DOPA and susceptibility in vivo; one study showed a decrease in 18F-DOPA PET in the posterior putamen was associated with iron accumulation in the lateral SN, as measured via R2* (Depierreux et al., 2021) (Fig. 3). This association and the localization of signal changes is thought to represent iron accumulation in the microglia due to inflammation and neuronal loss, further supporting a role of inflammation, oxidative stress, and neurodegeneration in the association of iron (QSM) and dopamine (F-dopa PET) signal (Depierreux et al., 2021; Wang et al., 2017). The method of evaluating associations of magnetic susceptibility and PET was unique in this study, as the imaging modalities were used to probe different brain regions and molecular

Author Manuscript Author Manuscript Author Manuscript Author Manuscript

aspects of PD, compared to other applications that primarily evaluate colocalization of signal changes.

3. Considerations in quantitative comparisons of QSM and PET

How the QSM data is acquired, processed, and used in analyses may affect study outcomes and the ability to detect associations with other imaging biomarkers or clinical metrics. Here we will review considerations relevant to comparisons with PET, which may also be applicable to comparisons with other imaging biomarkers.

First, one must consider co-registration of images in any multimodality comparison. Simultaneous PET-MR systems that allow for acquisition of PET and MR data in the same imaging session may facilitate co-registration. However, these systems are still relatively rare, especially in clinical settings. More commonly, patients receive PET-CT and MR imaging in separate sessions, often in close temporal proximity in the setting of a research protocol. Closer temporal spacing between the scans is critical, especially when the physiological processes imaged, such as neuroinflammation or metabolism, can change dynamically during the disease process. When the images are acquired on both modalities in the combined imaging session, the image co-registration is simplified as the patient is positioned similar in the scanner for both MR and PET. Even when acquired in the same session, co-registration between sequences should be performed to adjust for potential movement between sequences, particularly if smaller brain regions are investigated. In early PET/MR studies, attenuation correction posed challenges, but multiple MRI- and atlas-based methods have been validated across centers for brain imaging that are suitable for cross-modality investigations (Catana et al., 2022; Ladefoged et al., 2017).

Differences in QSM processing (phase unwrapping, masking, background field removal and inversion) may affect the QSM values generated (Vinayagamani et al., 2021; Wang and Liu, 2015). Details of and consensus recommendations for QSM processing are discussed in the article, *** by *** et al. in this special issue. Consistent use of the recommended acquisition protocol and processing pipeline will allow for more robust comparison of QSM-PET studies across sites in the future.

Once the QSM map is generated, one must decide how that data will be used, such as voxel-wise vs. ROI-based analyses and choice of a reference region (Fazlollahi et al., 2017a). Regional analyses are commonly used in QSM and PET studies, and the regions are selected based on structural anatomy (e.g. lobar regions of cortex and white matter, deep gray structures) and/or the disease process of interest. These regional approaches reduce noise but may also lose physiologic information with averaging of negative and positive values. Voxel-wise analyses may better reflect regional changes in diamagnetic and paramagnetic properties (negative and positive values) but are more susceptible to noise. Recent studies have proposed separate analysis of positive and negative QSM values (Chen et al., 2021a; Dimov et al., 2022; Emmerich et al., 2021; Shin et al., 2021); this approach could be considered in future PET comparison studies. Different selections of tissue reference (e.g. CSF, white matter, whole brain) may lead to different standard deviations of susceptibility in a region of interest. However, the reference region must be carefully chosen to reduce

Author Manuscript Author Manuscript Author Manuscript Author Manuscript

potential pathology-induced bias (Schweser et al., 2017; Straub et al., 2017). These topics are covered by a complimentary review article in this special issue.

Additional considerations in QSM-PET comparisons are differences in the magnitude of biologically relevant signal and noise properties for each image modality. For example, variation across individuals in QSM signal is much lower than that observed in amyloid and tau PET along the AD spectrum (Cogswell et al., 2021). In interpretation of statistical results, effect sizes and patterns of association may help inform clinical relevance of findings.

4. Conclusions and future directions

In conclusion, the study of the associations of magnetic susceptibility with PET markers of neurodegenerative diseases (Fig. 4) may help elucidate disease mechanisms. Current literature supports a role for inflammation and iron, as inferred by susceptibility, in parenchymal protein aggregation and neurodegeneration. Future PET tracer development and improvement in QSM acquisition and processing may provide further insight into these relationships, provide better understanding of QSM signal, and inform future applications for QSM in research and clinical practice.

Funding

There are no funding sources to report.

Data availability

No data was used for the research described in the article.

Abbreviations:

18F-DOPA	18F-fluorodopa
FDG	18F-fluorodeoxyglucose
TSPO	18-kDa translocator protein
ALS	Amyotrophic lateral sclerosis
AD	Alzheimer’s disease
CAA	Cerebral amyloid angiopathy
MS	Multiple sclerosis
PD	Parkinson’s disease
PET	Positron emission tomography
PSP	Progressive supranuclear palsy
QSM	Quantitative susceptibility mapping

Author Manuscript Author Manuscript Author Manuscript Author Manuscript

SVD	Small vessel disease

References

Acosta-Cabronero J, Betts MJ, Cardenas-Blanco A, Yang S, Nestor PJ, 2016. In vivo MRI mapping of brain iron deposition across the adult lifespan. J. Neurosci 36, 364–374. doi:10.1523/JNEUROSCI.1907-15.2016. [PubMed: 26758829]

Acosta-Cabronero J, Machts J, Schreiber S, Abdulla S, Kollewe K, Petri S, Spotorno N, Kaufmann J, Heinze H-J, Dengler R, Vielhaber S, Nestor PJ, 2018. Quantitative susceptibility MRI to detect brain iron in amyotrophic lateral sclerosis. Radiology 289, 195–203. doi:10.1148/radiol.2018180112. [PubMed: 30040038]

Alam MM, Lee J, Lee S-Y, 2017. Recent progress in the development of TSPO PET ligands for neuroinflammation imaging in neurological diseases. Nucl. Med. Mol. Imaging 51, 283–296. doi:10.1007/s13139-017-0475-8. [PubMed: 29242722]

Anazodo UC, Finger E, Kwan BYM, Pavlosky W, Warrington JC, Günther M, Prato FS, Thiessen JD, St Lawrence KS, 2018. Using simultaneous PET/MRI to compare the accuracy of diagnosing frontotemporal dementia by arterial spin labelling MRI and FDG-PET. Neuroimage Clin. 17, 405–414. doi:10.1016/j.nicl.2017.10.033. [PubMed: 29159053]

Ayton S, Fazlollahi A, Bourgeat P, Raniga P, Ng A, Lim YY, Diouf I, Farquharson S, Fripp J, Ames D, Doecke J, Desmond P, Ordidge R, Masters CL, Rowe CC, Maruff P, Villemagne VL, Salvado O, Bush AIAustralian Imaging Biomarkers and Lifestyle (AIBL) Research Group, 2017. Cerebral quantitative susceptibility mapping predicts amyloid-β-related cognitive decline. Brain 140, 2112–2119. doi:10.1093/brain/awx137. [PubMed: 28899019]

Ayton S, Wang Y, Diouf I, Schneider JA, Brockman J, Morris MC, Bush AI, 2019. Brain iron is associated with accelerated cognitive decline in people with Alzheimer pathology. Mol. Psychiatry 1–10. doi:10.1038/s41380-019-0375-7.

Baker SL, Harrison TM, Maass A, Joie RL, Jagust WJ, 2019. Effect of off-target binding on 18F-flortaucipir variability in healthy controls across the life span. J. Nucl. Med 60, 1444–1451. doi:10.2967/jnumed.118.224113. [PubMed: 30877180]

Berg RC, Preibisch C, Thomas DL, Shmueli K, Biondetti E, 2021. Investigating the effect of flow compensation and quantitative susceptibility mapping method on the accuracy of venous susceptibility measurement. Neuroimage 240, 118399. doi:10.1016/j.neuroimage.2021.118399. [PubMed: 34273528]

van Bergen JMG, Li X, Hua J, Schreiner SJ, Steininger SC, Quevenco FC, Wyss M, Gietl AF, Treyer V, Leh SE, Buck F, Nitsch RM, Pruessmann KP, van Zijl PCM, Hock C, Unschuld PG, 2016. Colocalization of cerebral iron with amyloid beta in mild cognitive impairment. Sci. Rep 6, 1–9. doi:10.1038/srep35514. [PubMed: 28442746]

Bilgic B, Pfefferbaum A, Rohlfing T, Sullivan EV, Adalsteinsson E, 2012. MRI estimates of brain iron concentration in normal aging using quantitative susceptibility mapping. Neuroimage 59, 2625–2635. doi:10.1016/j.neuroimage.2011.08.077. [PubMed: 21925274]

Braak H, Braak E, 1991. Neuropathological stageing of Alzheimer-related changes. Acta Neuropathol. 82, 239–259. doi:10.1007/BF00308809. [PubMed: 1759558]

Brendel M, Barthel H, van Eimeren T, Marek K, Beyer L, Song M, Palleis C, Gehmeyr M, Fietzek U, Respondek G, Sauerbeck J, Nitschmann A, Zach C, Hammes J, Barbe MT, Onur O, Jessen F, Saur D, Schroeter ML, Rumpf J-J, Rullmann M, Schildan A, Patt M, Neumaier B, Barret O, Madonia J, Russell DS, Stephens A, Roeber S, Herms J, Bötzel K, Classen J, Bartenstein P, Villemagne V, Levin J, Höglinger GU, Drzezga A, Seibyl J, Sabri O, 2020. Assessment of 18F-PI-2620 as a biomarker in progressive supranuclear palsy. JAMA Neurol. 77, 1–13. doi:10.1001/jamaneurol.2020.2526. [PubMed: 32614385]

Carlson ML, Park J-H, Lieb T, James ML, 2020. TSPO-PET/MRI reveals increased neuroinflammation in basal ganglia of chronic fatigue syndrome patients. ISMRM & SMRT Virtual Conference & Exhibition. Presented at the ISMRM & SMRT Virtual Conference & Exhibition.

Author Manuscript Author Manuscript Author Manuscript Author Manuscript

Catana C, Laforest R, An H, Boada F, Cao T, Faul D, Jakoby B, Jansen FP, Kemp BJ, Kinahan PE, Larson P, Levine MA, Maniawski P, Mawlawi O, McConathy JE, McMillan AB, Price JC, Rajagopal A, Sunderland J, Veit-Haibach P, Wangerin KA, Ying C, Hope TA, 2022. A path to qualification of PET/MRI scanners for multicenter brain imaging studies: evaluation of MRI-based attenuation correction methods using a patient phantom. J. Nucl. Med 63, 615–621. doi:10.2967/jnumed.120.261881. [PubMed: 34301784]

Ceccarini J, Bourgeois S, Van Weehaeghe D, Goffin K, Vandenberghe R, Vandenbulcke M, Sunaert S, Van Laere K, 2020. Direct prospective comparison of 18F-FDG PET and arterial spin labelling MR using simultaneous PET/MR in patients referred for diagnosis of dementia. Eur. J. Nucl. Med. Mol. Imaging 47, 2142–2154. doi:10.1007/s00259-020-04694-1. [PubMed: 31960098]

Chandra A, Valkimadi P-E, Pagano G, Cousins O, Dervenoulas G, Politis MAlzheimer's Disease Neuroimaging Initiative, 2019. Applications of amyloid, tau, and neuroinflammation PET imaging to Alzheimer's disease and mild cognitive impairment. Hum. Brain Mapp 40, 5424–5442. doi:10.1002/hbm.24782. [PubMed: 31520513]

Charidimou A, Farid K, Baron J-C, 2017. Amyloid-PET in sporadic cerebral amyloid angiopathy: a diagnostic accuracy meta-analysis. Neurology 89, 1490–1498. doi:10.1212/WNL.0000000000004539. [PubMed: 28855406]

Charidimou A, Gang Q, Werring DJ, 2012. Sporadic cerebral amyloid angiopathy revisited: recent insights into pathophysiology and clinical spectrum. J. Neurol. Neurosurg. Psychiatry 83, 124–137. doi:10.1136/jnnp-2011-301308. [PubMed: 22056963]

Chen J, Gong N-J, Chaim KT, Otaduy MCG, Liu C, 2021a. Decompose quantitative susceptibility mapping (QSM) to sub-voxel diamagnetic and paramagnetic components based on gradient-echo MRI data. Neuroimage 242, 118477. doi:10.1016/j.neuroimage.2021.118477. [PubMed: 34403742]

Chen L, Soldan A, Oishi K, Faria A, Zhu Y, Albert M, van Zijl PCM, Li X, 2021b. Quantitative susceptibility mapping of brain iron and β-amyloid in MRI and PET relating to cognitive performance in cognitively normal older adults. Radiology 298, 353–362. doi:10.1148/radiol.2020201603. [PubMed: 33231528]

Chen M-K, Mecca AP, Naganawa M, Gallezot J-D, Toyonaga T, Mondal J, Finnema SJ, Lin S-F, O'Dell RS, McDonald JW, Michalak HR, Vander Wyk B, Nabulsi NB, Huang Y, Arnsten AF, van Dyck CH, Carson RE, 2021c. Comparison of [11C]UCB-J and [18F]FDG PET in Alzheimer's disease: a tracer kinetic modeling study. J. Cereb. Blood Flow Metab 41, 2395–2409. doi:10.1177/0271678X211004312. [PubMed: 33757318]

Chételat G, Arbizu J, Barthel H, Garibotto V, Law I, Morbelli S, van de Giessen E, Agosta F, Barkhof F, Brooks DJ, Carrillo MC, Dubois B, Fjell AM, Frisoni GB, Hansson O, Herholz K, Hutton BF, Jack CR, Lammertsma AA, Landau SM, Minoshima S, Nobili F, Nordberg A, Ossenkoppele R, Oyen WJG, Perani D, Rabinovici GD, Scheltens P, Villemagne VL, Zetterberg H, Drzezga A, 2020. Amyloid-PET and 18F-FDG-PET in the diagnostic investigation of Alzheimer's disease and other dementias. Lancet Neurol. 19, 951–962. doi:10.1016/S1474-4422(20)30314-8. [PubMed: 33098804]

Chew S, Atassi N, 2019. Positron emission tomography molecular imaging biomarkers for amyotrophic lateral sclerosis. Front. Neurol 10, 135. doi:10.3389/fneur.2019.00135. [PubMed: 30881332]

Cho J, Kee Y, Spincemaille P, Nguyen TD, Zhang J, Gupta A, Zhang S, Wang Y, 2018. Cerebral metabolic rate of oxygen (CMRO2) mapping by combining quantitative susceptibility mapping (QSM) and quantitative blood oxygenation level-dependent imaging (qBOLD). Magn. Reson. Med 80, 1595–1604. doi:10.1002/mrm.27135. [PubMed: 29516537]

Cho J, Lee J, An H, Goyal MS, Su Y, Wang Y, 2021. Cerebral oxygen extraction fraction (OEF): comparison of challenge-free gradient echo QSM+qBOLD (QQ) with 15O PET in healthy adults. J. Cereb. Blood Flow Metab 41, 1658–1668. doi:10.1177/0271678X20973951. [PubMed: 33243071]

Choi JY, Cho H, Ahn SJ, Lee JH, Ryu YH, Lee MS, Lyoo CH, 2018. Off-target 18F-AV-1451 binding in the basal ganglia correlates with age-related iron accumulation. J. Nucl. Med 59, 117–120. doi:10.2967/jnumed.117.195248. [PubMed: 28775201]

Author Manuscript Author Manuscript Author Manuscript Author Manuscript

Cogswell PM, Wiste HJ, Senjem ML, Gunter JL, Weigand SD, Schwarz CG, Arani A, Therneau TM, Lowe VJ, Knopman DS, Botha H, Graff-Radford J, Jones DT, Kantarci K, Vemuri P, Boeve BF, Mielke MM, Petersen RC, Jack CR, 2021. Associations of quantitative susceptibility mapping with Alzheimer's disease clinical and imaging markers. Neuroimage 224, 117433. doi:10.1016/j.neuroimage.2020.117433. [PubMed: 33035667]

Collij LE, Salvadó G, Wottschel V, Mastenbroek SE, Schoenmakers P, Heeman F, Aksman L, Wink AM, Berckel BNM, van de Flier WM, Scheltens P, Visser PJ, Barkhof F, Haller S, Gispert JD, Alves IL Initiative, for the A.D.N., Study, for the A., 2022. Spatial-temporal patterns of β-amyloid accumulation: a subtype and stage inference model analysis. Neurology 98, e1692–e1703. doi:10.1212/WNL.0000000000200148. [PubMed: 35292558]

Collingwood JF, Mikhaylova A, Davidson M, Batich C, Streit WJ, Terry J, Dobson J, 2005. In situ characterization and mapping of iron compounds in Alzheimer's disease tissue. J. Alzheimer's Dis 7, 267–272. doi:10.3233/JAD-2005-7401. [PubMed: 16131727]

Cummings J, Rabinovici GD, Atri A, Aisen P, Apostolova LG, Hendrix S, Sabbagh M, Selkoe D, Weiner M, Salloway SAlzheimer's Disease and Related Disorders Therapeutics Working Group, 2022. Aducanumab: appropriate use recommendations update. J. Prev. Alzheimers Dis doi:10.14283/jpad.2022.34.

Dani M, Wood M, Mizoguchi R, Fan Z, Walker Z, Morgan R, Hinz R, Biju M, Kuruvilla T, Brooks DJ, Edison P, 2018. Microglial activation correlates in vivo with both tau and amyloid in Alzheimer's disease. Brain 141, 2740–2754. doi:10.1093/brain/awy188. [PubMed: 30052812]

de Rochefort L, Brown R, Prince MR, Wang Y, 2008. Quantitative MR susceptibility mapping using piece-wise constant regularized inversion of the magnetic field. Magn. Reson. Med 60, 1003–1009. doi:10.1002/mrm.21710. [PubMed: 18816834]

Deibel MA, Ehmann WD, Markesbery WR, 1996. Copper, iron, and zinc imbalances in severely degenerated brain regions in Alzheimer's disease: possible relation to oxidative stress. J. Neurol. Sci 143, 137–142. doi:10.1016/S0022-510X(96)00203-1. [PubMed: 8981312]

Deistung A, Schäfer A, Schweser F, Biedermann U, Turner R, Reichenbach JR, 2013. Toward in vivo histology: a comparison of quantitative susceptibility mapping (QSM) with magnitude-, phase-, and R2*-imaging at ultra-high magnetic field strength. Neuroimage 65, 299–314. doi:10.1016/j.neuroimage.2012.09.055. [PubMed: 23036448]

Depierreux F, Parmentier E, Mackels L, Baquero K, Degueldre C, Balteau E, Salmon E, Phillips C, Bahri MA, Maquet P, Garraux G, 2021. Parkinson's disease multimodal imaging: F-DOPA PET, neuromelanin-sensitive and quantitative iron-sensitive MRI. npj Parkinsons Dis. 7, 1–10. doi:10.1038/s41531-021-00199-2. [PubMed: 33397996]

Derry PJ, Kent TA, 2017. Correlating quantitative susceptibility mapping with cognitive decline in Alzheimer's disease. Brain 140, 2069–2072. doi:10.1093/brain/awx167. [PubMed: 28899022]

Dimov AV, Nguyen TD, Gillen KM, Marcille M, Spincemaille P, Pitt D, Gauthier SA, Wang Y, 2022. Susceptibility source separation from gradient echo data using magnitude decay modeling. J. Neuroimaging 32, 852–859. doi:10.1111/jon.13014. [PubMed: 35668022]

Dixon SJ, Lemberg KM, Lamprecht MR, Skouta R, Zaitsev EM, Gleason CE, Patel DN, Bauer AJ, Cantley AM, Yang WS, Morrison B, Stockwell BR, 2012. Ferroptosis: an iron-dependent form of nonapoptotic cell death. Cell 149, 1060–1072. doi:10.1016/j.cell.2012.03.042. [PubMed: 22632970]

Du G, Liu T, Lewis MM, Kong L, Wang Y, Connor J, Mailman RB, Huang X, 2016. Quantitative susceptibility mapping of the midbrain in Parkinson's disease. Mov. Disord 31, 317–324. doi:10.1002/mds.26417. [PubMed: 26362242]

Emmerich J, Bachert P, Ladd ME, Straub S, 2021. On the separation of susceptibility sources in quantitative susceptibility mapping: theory and phantom validation with an in vivo application to multiple sclerosis lesions of different age. J. Magn. Reson 330, 107033. doi:10.1016/j.jmr.2021.107033. [PubMed: 34303117]

Everett J, Céspedes E, Shelford LR, Exley C, Collingwood JF, Dobson J, van der Laan G, Jenkins CA, Arenholz E, Telling ND, 2014. Ferrous iron formation following the co-aggregation of ferric iron and the Alzheimer's disease peptide β-amyloid (1–42). J. R. Soc. Interface 11, 20140165. doi:10.1098/rsif.2014.0165. [PubMed: 24671940]

Author Manuscript Author Manuscript Author Manuscript Author Manuscript

Fan AP, Bilgic B, Gagnon L, Witzel T, Bhat H, Rosen BR, Adalsteinsson E, 2014. Quantitative oxygenation venography from MRI phase. Magn. Reson. Med 72, 149–159. doi:10.1002/mrm.24918. [PubMed: 24006229]

Fazlollahi A, Ayton S, Bourgeat P, Raniga P, Ng A, Fripp J, Ames D, Masters CL, Rowe CC, Villemagne VL, Bush AI, Salvado O, 2017a. A normalisation framework for quantitative brain imaging; application to quantitative susceptibility mapping. In: 2017 IEEE 14th International Symposium on Biomedical Imaging (ISBI 2017). Presented at the 2017 IEEE 14th International Symposium on Biomedical Imaging (ISBI 2017), pp. 97–100. doi:10.1109/ISBI.2017.7950477.

Fazlollahi A, Ayton S, Diouf I, Bourgeat P, Raniga P, Dore V, Ng A, Fripp J, Ames D, Masters CL, Rowe CC, Villemagne VL, Bush AI, Salvado O, 2017b. Quantitative susceptibility mapping of the hippocampus predicts hippocampal atrophy in Aβ+ elderly controls and Alzheimer's disease patients. Alzheimer's Dement. 13, P454–P455. doi:10.1016/j.jalz.2017.06.460.

Fujita M, Kobayashi M, Ikawa M, Gunn RN, Rabiner EA, Owen DR, Zoghbi SS, Haskali MB, Telu S, Pike VW, Innis RB, 2017. Comparison of four 11C-labeled PET ligands to quantify translocator protein 18 kDa (TSPO) in human brain: (R)-PK11195, PBR28, DPA-713, and ER176-based on recent publications that measured specific-to-non-displaceable ratios. EJNMMI Res. 7, 84. doi:10.1186/s13550-017-0334-8. [PubMed: 29038960]

Garnett ES, Firnau G, Nahmias C, 1983. Dopamine visualized in the basal ganglia of living man. Nature 305, 137–138. doi:10.1038/305137a0. [PubMed: 6604227]

Gong N-J, Dibb R, Bulk M, van der Weerd L, Liu C, 2019. Imaging beta amyloid aggregation and iron accumulation in Alzheimer's disease using quantitative susceptibility mapping MRI. Neuroimage 191, 176–185. doi:10.1016/j.neuroimage.2019.02.019. [PubMed: 30739060]

Gouilly D, Saint-Aubert L, Ribeiro M-J, Salabert A-S, Tauber C, Péran P, Arlicot N, Pariente J, Payoux P, 2022. Neuroinflammation PET imaging of the translocator protein (TSPO) in Alzheimer's disease: an update. Eur. J. Neurosci 55, 1322–1343. doi:10.1111/ejn.15613. [PubMed: 35083791]

Greenberg SM, Bacskai BJ, Hernandez-Guillamon M, Pruzin J, Sperling R, van Veluw SJ, 2020. Cerebral amyloid angiopathy and Alzheimer disease—One peptide, two pathways. Nat. Rev. Neurol 16, 30–42. doi:10.1038/s41582-019-0281-2. [PubMed: 31827267]

Greenberg SM, Charidimou A, 2018. Diagnosis of cerebral amyloid angiopathy. Stroke 49, 491–497. doi:10.1161/STROKEAHA.117.016990. [PubMed: 29335334]

Greenberg SM, Grabowski T, Gurol ME, Skehan ME, Nandigam RNK, Becker JA, Garcia-Alloza M, Prada C, Frosch MP, Rosand J, Viswanathan A, Smith EE, Johnson KA, 2008. Detection of isolated cerebrovascular beta-amyloid with Pittsburgh compound B. Ann. Neurol 64, 587–591. doi:10.1002/ana.21528. [PubMed: 19067370]

Grothe MJ, Barthel H, Sepulcre J, Dyrba M, Sabri O, Teipel SJAlzheimer's Disease Neuroimaging Initiative, 2017. In vivo staging of regional amyloid deposition. Neurology 89, 2031–2038. doi:10.1212/WNL.0000000000004643. [PubMed: 29046362]

Haacke EM, Liu S, Buch S, Zheng W, Wu D, Ye Y, 2015. Quantitative susceptibility mapping: current status and future directions. Magn. Reson. Imaging 33, 1–25. doi:10.1016/j.mri.2014.09.004. [PubMed: 25267705]

Harada R, Ishiki A, Kai H, Sato N, Furukawa K, Furumoto S, Tago T, Tomita N, Watanuki S, Hiraoka K, Ishikawa Y, Funaki Y, Nakamura T, Yoshikawa T, Iwata R, Tashiro M, Sasano H, Kitamoto T, Yanai K, Arai H, Kudo Y, Okamura N, 2018. Correlations of 18F-THK5351 PET with postmortem burden of tau and astrogliosis in Alzheimer disease. J. Nucl. Med 59, 671–674. doi:10.2967/jnumed.117.197426. [PubMed: 28864633]

Hashimoto M, Hsu LJ, Xia Y, Takeda A, Sisk A, Sundsmo M, Masliah E, 1999. Oxidative stress induces amyloid-like aggregate formation of NACP/alpha-synuclein in vitro. Neuroreport 10, 717–721. doi:10.1097/00001756-199903170-00011. [PubMed: 10208537]

Hautot D, Pankhurst QA, Khan N, Dobson J, 2003. Preliminary evaluation of nanoscale biogenic magnetite in Alzheimer's disease brain tissue. Proc. Biol. Sci 270, S62–S64. doi:10.1098/rsbl.2003.0012. [PubMed: 12952638]

He N, Ling H, Ding B, Huang J, Zhang Y, Zhang Z, Liu C, Chen K, Yan F, 2015. Region-specific disturbed iron distribution in early idiopathic Parkinson's disease measured by quantitative

Author Manuscript Author Manuscript Author Manuscript Author Manuscript

susceptibility mapping. Hum. Brain Mapp 36, 4407–4420. doi:10.1002/hbm.22928. [PubMed: 26249218]

Heiss W-D, 2018. The additional value of PET in the assessment of cerebral small vessel disease. J. Nucl. Med 59, 1660–1664. doi:10.2967/jnumed.118.214270. [PubMed: 29959217]

Herranz E, Louapre C, Treaba CA, Govindarajan ST, Ouellette R, Mangeat G, Loggia ML, Cohen-Adad J, Klawiter EC, Sloane JA, Mainero C, 2020. Profiles of cortical inflammation in multiple sclerosis by 11C-PBR28 MR-PET and 7 Tesla imaging. Mult. Scler 26, 1497–1509. doi:10.1177/1352458519867320. [PubMed: 31368404]

Hooker JM, Carson RE, 2019. Human positron emission tomography neuroimaging. Annu. Rev. Biomed. Eng 21, 551–581. doi:10.1146/annurev-bioeng-062117-121056. [PubMed: 31167104]

Hyman BT, Phelps CH, Beach TG, Bigio EH, Cairns NJ, Carrillo MC, Dickson DW, Duyckaerts C, Frosch MP, Masliah E, Mirra SS, Nelson PT, Schneider JA, Thal DR, Thies B, Trojanowski JQ, Vinters HV, Montine TJ, 2012. National Institute on aging-Alzheimer's association guidelines for the neuropathologic assessment of Alzheimer's disease. Alzheimers Dement. 8, 1–13. doi:10.1016/j.jalz.2011.10.007. [PubMed: 22265587]

Ikawa M, Okazawa H, Tsujikawa T, Matsunaga A, Yamamura O, Mori T, Hamano T, Kiyono Y, Nakamoto Y, Yoneda M, 2015. Increased oxidative stress is related to disease severity in the ALS motor cortex: a PET study. Neurology 84, 2033–2039. doi:10.1212/WNL.0000000000001588. [PubMed: 25904686]

Ishii K, Kitagaki H, Kono M, Mori E, 1996. Decreased medial temporal oxygen metabolism in Alzheimer's disease shown by PET. J. Nucl. Med 37, 1159–1165. [PubMed: 8965188]

Jack CR, Bennett DA, Blennow K, Carrillo MC, Dunn B, Haeberlein SB, Holtzman DM, Jagust W, Jessen F, Karlawish J, Liu E, Molinuevo JL, Montine T, Phelps C, Rankin KP, Rowe CC, Scheltens P, Siemers E, Snyder HM, Sperling RContributors, 2018. NIA-AA research framework: toward a biological definition of Alzheimer's disease. Alzheimers Dement. 14, 535–562. doi:10.1016/j.jalz.2018.02.018. [PubMed: 29653606]

Jack CR, Garwood M, Wengenack TM, Borowski B, Curran GL, Lin J, Adriany G, Gröhn OHJ, Grimm R, Poduslo JF, 2004. In vivo visualization of Alzheimer's amyloid plaques by magnetic resonance imaging in transgenic mice without a contrast agent. Magn. Reson. Med 52, 1263–1271. doi:10.1002/mrm.20266. [PubMed: 15562496]

Jack CR, Wiste HJ, Weigand SD, Therneau TM, Lowe VJ, Knopman DS, Gunter JL, Senjem ML, Jones DT, Kantarci K, Machulda MM, Mielke MM, Roberts RO, Vemuri P, Reyes DA, Petersen RC, 2017. Defining imaging biomarker cut points for brain aging and Alzheimer's disease. Alzheimers Dement. 13, 205–216. doi:10.1016/j.jalz.2016.08.005. [PubMed: 27697430]

Janelidze S, Mattsson N, Palmqvist S, Smith R, Beach TG, Serrano GE, Chai X, Proctor NK, Eichenlaub U, Zetterberg H, Blennow K, Reiman EM, Stomrud E, Dage JL, Hansson O, 2020. Plasma P-tau181 in Alzheimer's disease: relationship to other biomarkers, differential diagnosis, neuropathology and longitudinal progression to Alzheimer's dementia. Nat. Med 26, 379–386. doi:10.1038/s41591-020-0755-1. [PubMed: 32123385]

Janelidze S, Teunissen CE, Zetterberg H, Allué JA, Sarasa L, Eichenlaub U, Bittner T, Ovod V, Verberk IMW, Toba K, Nakamura A, Bateman RJ, Blennow K, Hansson O, 2021. Head-to-head comparison of 8 plasma amyloid-β 42/40 assays in Alzheimer disease. JAMA Neurol. 78, 1375–1382. doi:10.1001/jamaneurol.2021.3180. [PubMed: 34542571]

Jelistratova I, Teipel SJ, Grothe MJ, 2020. Longitudinal validity of PET-based staging of regional amyloid deposition. Hum. Brain Mapp 41, 4219–4231. doi:10.1002/hbm.25121. [PubMed: 32648624]

Jiang D, Lin Z, Liu P, Sur S, Xu C, Hazel K, Pottanat G, Darrow J, Pillai JJ, Yasar S, Rosenberg P, Moghekar A, Albert M, Lu H, 2020. Brain oxygen extraction is differentially altered by Alzheimer's and vascular diseases. J. Magn. Reson. Imaging 52, 1829–1837. doi:10.1002/jmri.27264. [PubMed: 32567195]

Johnson KA, Gregas M, Becker JA, Kinnecom C, Salat DH, Moran EK, Smith EE, Rosand J, Rentz DM, Klunk WE, Mathis CA, Price JC, Dekosky ST, Fischman AJ, Greenberg SM, 2007. Imaging of amyloid burden and distribution in cerebral amyloid angiopathy. Ann. Neurol 62, 229–234. doi:10.1002/ana.21164. [PubMed: 17683091]

Author Manuscript Author Manuscript Author Manuscript Author Manuscript

Johnson KA, Minoshima S, Bohnen NI, Donohoe KJ, Foster NL, Herscovitch P, Karlawish JH, Rowe CC, Hedrick S, Pappas V, Carrillo MC, Hartley DM, 2013. Update on appropriate use criteria for amyloid PET imaging: dementia experts, mild cognitive impairment, and education. J. Nucl. Med 54, 1011–1013. doi:10.2967/jnumed.113.127068. [PubMed: 23753186]

Johnson KA, Schultz A, Betensky RA, Becker JA, Sepulcre J, Rentz D, Mormino E, Chhatwal J, Amariglio R, Papp K, Marshall G, Albers M, Mauro S, Pepin L, Alverio J, Judge K, Philiossaint M, Shoup T, Yokell D, Dickerson B, Gomez-Isla T, Hyman B, Vasdev N, Sperling R, 2016. Tau positron emission tomographic imaging in aging and early Alzheimer disease. Ann. Neurol 79, 110–119. doi:10.1002/ana.24546. [PubMed: 26505746]

Kaunzner UW, Kang Y, Zhang S, Morris E, Yao Y, Pandya S, Hurtado Rua SM, Park C, Gillen KM, Nguyen TD, Wang Y, Pitt D, Gauthier SA, 2019. Quantitative susceptibility mapping identifies inflammation in a subset of chronic multiple sclerosis lesions. Brain 142, 133–145. doi:10.1093/brain/awy296. [PubMed: 30561514]

Kaur D, Sharma V, Deshmukh R, 2019. Activation of microglia and astrocytes: a roadway to neuroinflammation and Alzheimer's disease. Inflammopharmacology 27, 663–677. doi:10.1007/s10787-019-00580-x. [PubMed: 30874945]

Kim H-G, Park S, Rhee HY, Lee KM, Ryu C-W, Rhee SJ, Lee SY, Wang Y, Jahng G-H, 2017. Quantitative susceptibility mapping to evaluate the early stage of Alzheimer's disease. Neuroimage Clin. 16, 429–438. doi:10.1016/j.nicl.2017.08.019. [PubMed: 28879084]

Klunk WE, Engler H, Nordberg A, Wang Y, Blomqvist G, Holt DP, Bergström M, Savitcheva I, Huang G, Estrada S, Ausén B, Debnath ML, Barletta J, Price JC, Sandell J, Lopresti BJ, Wall A, Koivisto P, Antoni G, Mathis CA, Långström B, 2004. Imaging brain amyloid in Alzheimer's disease with Pittsburgh compound-B. Ann. Neurol 55, 306–319. doi:10.1002/ana.20009. [PubMed: 14991808]

Knezevic D, Mizrahi R, 2018. Molecular imaging of neuroinflammation in Alzheimer's disease and mild cognitive impairment. Prog. Neuropsychopharmacol. Biol. Psychiatry 80, 123–131. doi:10.1016/j.pnpbp.2017.05.007. [PubMed: 28533150]

Kwan JY, Jeong SY, Van Gelderen P, Deng H-X, Quezado MM, Danielian LE, Butman JA, Chen L, Bayat E, Russell J, Siddique T, Duyn JH, Rouault TA, Floeter MK, 2012. Iron accumulation in deep cortical layers accounts for MRI signal abnormalities in ALS: correlating 7 Tesla MRI and pathology. PLoS One 7, e35241. doi:10.1371/journal.pone.0035241. [PubMed: 22529995]

Kwon HS, Koh S-H, 2020. Neuroinflammation in neurodegenerative disorders: the roles of microglia and astrocytes. Transl. Neurodegener 9, 42. doi:10.1186/s40035-020-00221-2. [PubMed: 33239064]

Ladefoged CN, Law I, Anazodo U, St Lawrence K, Izquierdo-Garcia D, Catana C, Burgos N, Cardoso MJ, Ourselin S, Hutton B, Mérida I, Costes N, Hammers A, Benoit D, Holm S, Juttukonda M, An H, Cabello J, Lukas M, Nekolla S, Ziegler S, Fenchel M, Jakoby B, Casey ME, Benzinger T, Højgaard L, Hansen AE, Andersen FL, 2017. A multi-centre evaluation of eleven clinically feasible brain PET/MRI attenuation correction techniques using a large cohort of patients. Neuroimage 147, 346–359. doi:10.1016/j.neuroimage.2016.12.010. [PubMed: 27988322]

Lagarde J, Sarazin M, Bottlaender M, 2018. In vivo PET imaging of neuroinflammation in Alzheimer's disease. J. Neural. Transm. (Vienna) 125, 847–867. doi:10.1007/s00702-017-1731-x. [PubMed: 28516240]

Lane DJR, Ayton S, Bush AI, 2018. Iron and Alzheimer's disease: an update on emerging mechanisms. J. Alzheimers Dis 64, S379–S395. doi:10.3233/JAD-179944. [PubMed: 29865061]

Lassmann H, van Horssen J, 2011. The molecular basis of neurodegeneration in multiple sclerosis. FEBS Lett. 585, 3715–3723. doi:10.1016/j.febslet.2011.08.004. [PubMed: 21854776]

Lavisse S, Guillermier M, Hérard A-S, Petit F, Delahaye M, Van Camp N, Ben Haim L, Lebon V, Remy P, Dollé F, Delzescaux T, Bonvento G, Hantraye P, Escartin C, 2012. Reactive astrocytes overexpress TSPO and are detected by TSPO positron emission tomography imaging. J. Neurosci 32, 10809–10818. doi:10.1523/JNEUROSCI.1487-12.2012. [PubMed: 22875916]

Lee K, Ellison B, Selim M, Long NH, Filippidis A, Thomas AJ, Spincemaille P, Wang Y, Soman S, 2022. Quantitative susceptibility mapping improves cerebral microbleed detection relative to susceptibility-weighted images. J. Neuroimaging doi:10.1111/jon.13054.

Author Manuscript Author Manuscript Author Manuscript Author Manuscript

Lemoine L, Leuzy A, Chiotis K, Rodriguez-Vieitez E, Nordberg A, 2018. Tau positron emission tomography imaging in tauopathies: the added hurdle of off-target binding. Alzheimers Dement. (Amst) 10, 232–236. doi:10.1016/j.dadm.2018.01.007. [PubMed: 29780868]

Leuzy A, Chiotis K, Lemoine L, Gillberg P-G, Almkvist O, Rodriguez-Vieitez E, Nordberg A, 2019. Tau PET imaging in neurodegenerative tauopathies-still a challenge. Mol. Psychiatry 24, 1112–1134. doi:10.1038/s41380-018-0342-8. [PubMed: 30635637]

Li J, Cao F, Yin H, Huang Z, Lin Z, Mao N, Sun B, Wang G, 2020. Ferroptosis: past, present and future. Cell Death Dis. 11, 1–13. doi:10.1038/s41419-020-2298-2. [PubMed: 31911576]

Li W, Wu B, Batrachenko A, Bancroft-Wu V, Morey RA, Shashi V, Langkammer C, De Bellis MD, Ropele S, Song AW, Liu C, 2014. Differential developmental trajectories of magnetic susceptibility in human brain gray and white matter over the lifespan. Hum. Brain Mapp 35, 2698–2713. doi:10.1002/hbm.22360. [PubMed: 24038837]

Li W, Wu B, Liu C, 2011. Quantitative susceptibility mapping of human brain reflects spatial variation in tissue composition. Neuroimage 55, 1645–1656. doi:10.1016/j.neuroimage.2010.11.088. [PubMed: 21224002]

Liddelow SA, Guttenplan KA, Clarke LE, Bennett FC, Bohlen CJ, Schirmer L, Bennett ML, Münch AE, Chung W-S, Peterson TC, Wilton DK, Frouin A, Napier BA, Panicker N, Kumar M, Buckwalter MS, Rowitch DH, Dawson VL, Dawson TM, Stevens B, Barres BA, 2017. Neurotoxic reactive astrocytes are induced by activated microglia. Nature 541, 481–487. doi:10.1038/nature21029. [PubMed: 28099414]

Lister-James J, Pontecorvo MJ, Clark C, Joshi AD, Mintun MA, Zhang W, Lim N, Zhuang Z, Golding G, Choi SR, Benedum TE, Kennedy P, Hefti F, Carpenter AP, Kung HF, Skovronsky DM, 2011. Florbetapir f-18: a histopathologically validated beta-amyloid positron emission tomography imaging agent. Semin. Nucl. Med 41, 300–304. doi:10.1053/j.semnuclmed.2011.03.001. [PubMed: 21624563]

Liu C, Li W, Tong KA, Yeom KW, Kuzminski S, 2015. Susceptibility-weighted imaging and quantitative susceptibility mapping in the brain. J. Magn. Reson. Imaging 42, 23–41. doi:10.1002/jmri.24768. [PubMed: 25270052]

Loane C, Politis M, 2011. Positron emission tomography neuroimaging in Parkinson's disease. Am. J. Transl. Res 3, 323–341. [PubMed: 21904653]

Lois C, Gonzalez I, Johnson KA, Price JC, 2019. PET imaging of tau protein targets: a methodology perspective. Brain Imaging Behav. 13, 333–344. doi:10.1007/s11682-018-9847-7. [PubMed: 29497982]

Meadowcroft MD, Connor JR, Smith MB, Yang QX, 2009. MRI and histological analysis of beta-amyloid plaques in both human Alzheimer's disease and APP/PS1 transgenic mice. J. Magn. Reson. Imaging 29, 997–1007. doi:10.1002/jmri.21731. [PubMed: 19388095]

Mielke MM, Frank RD, Dage JL, Jeromin A, Ashton NJ, Blennow K, Karikari TK, Vanmechelen E, Zetterberg H, Algeciras-Schimnich A, Knopman DS, Lowe V, Bu G, Vemuri P, Graff-Radford J, Jack CR Jr, Petersen RC, 2021. Comparison of plasma phosphorylated tau species with amyloid and tau positron emission tomography, neurodegeneration, vascular pathology, and cognitive outcomes. JAMA Neurol. 78, 1108–1117. doi:10.1001/jamaneurol.2021.2293. [PubMed: 34309632]

Mielke MM, Hagen CE, Xu J, Chai X, Vemuri P, Lowe VJ, Airey DC, Knopman DS, Roberts RO, Machulda MM, Jack CR, Petersen RC, Dage JL, 2018. Plasma phospho-tau181 increases with Alzheimer's disease clinical severity and is associated with tau-PET and amyloid-PET. Alzheimers Dement. 14, 989–997. doi:10.1016/j.jalz.2018.02.013. [PubMed: 29626426]

Minoshima S, Mosci K, Cross D, Thientunyakit T, 2021. Brain [F-18]FDG PET for clinical dementia workup: differential diagnosis of Alzheimer's disease and other types of dementing disorders. Semin Nucl. Med 51, 230–240. doi:10.1053/j.semnuclmed.2021.01.002. [PubMed: 33546814]

Mintun MA, Larossa GN, Sheline YI, Dence CS, Lee SY, Mach RH, Klunk WE, Mathis CA, DeKosky ST, Morris JC, 2006. [11C]PIB in a nondemented population: potential antecedent marker of Alzheimer disease. Neurology 67, 446–452. doi:10.1212/01.wnl.0000228230.26044.a4. [PubMed: 16894106]

Author Manuscript Author Manuscript Author Manuscript Author Manuscript

Moon Y, Han S-H, Moon W-J, 2016. Patterns of brain iron accumulation in vascular dementia and Alzheimer's dementia using quantitative susceptibility mapping imaging. J. Alzheimers Dis 51, 737–745. doi:10.3233/JAD-151037. [PubMed: 26890777]

Morrish PK, Sawle GV, Brooks DJ, 1996. An [18F]dopa-PET and clinical study of the rate of progression in Parkinson's disease. Brain 119 (Pt 2), 585–591. doi:10.1093/brain/119.2.585. [PubMed: 8800950]

Mosconi L, Mistur R, Switalski R, Tsui WH, Glodzik L, Li Y, Pirraglia E, De Santi S, Reisberg B, Wisniewski T, de Leon MJ, 2009. FDG-PET changes in brain glucose metabolism from normal cognition to pathologically verified Alzheimer's disease. Eur. J. Nucl. Med. Mol. Imaging 36, 811–822. doi:10.1007/s00259-008-1039-z. [PubMed: 19142633]

Mosconi L, Tsui WH, Herholz K, Pupi A, Drzezga A, Lucignani G, Reiman EM, Holthoff V, Kalbe E, Sorbi S, Diehl-Schmid J, Perneczky R, Clerici F, Caselli R, Beuthien-Baumann B, Kurz A, Minoshima S, de Leon MJ, 2008. Multicenter standardized 18F-FDG PET diagnosis of mild cognitive impairment, Alzheimer's disease, and other dementias. J. Nucl. Med 49, 390–398. doi:10.2967/jnumed.107.045385. [PubMed: 18287270]

Murakami Y, Kakeda S, Watanabe K, Ueda I, Ogasawara A, Moriya J, Ide S, Futatsuya K, Sato T, Okada K, Uozumi T, Tsuji S, Liu T, Wang Y, Korogi Y, 2015. Usefulness of quantitative susceptibility mapping for the diagnosis of Parkinson disease. AJNR Am. J. Neuroradiol 36, 1102–1108. doi:10.3174/ajnr.A4260. [PubMed: 25767187]

Ndayisaba A, Kaindlstorfer C, Wenning GK, 2019. Iron in neurodegeneration - cause or consequence? Front. Neurosci 13, 180. doi:10.3389/fnins.2019.00180. [PubMed: 30881284]

Nnah IC, Wessling-Resnick M, 2018. Brain iron homeostasis: a focus on microglial iron. Pharmaceuticals (Basel) 11, 129. doi:10.3390/ph11040129. [PubMed: 30477086]

Ossenkoppele R, Schonhaut DR, Schöll M, Lockhart SN, Ayakta N, Baker SL, O'Neil JP, Janabi M, Lazaris A, Cantwell A, Vogel J, Santos M, Miller ZA, Bettcher BM, Vossel KA, Kramer JH, Gorno-Tempini ML, Miller BL, Jagust WJ, Rabinovici GD, 2016. Tau PET patterns mirror clinical and neuroanatomical variability in Alzheimer's disease. Brain 139, 1551–1567. doi:10.1093/brain/aww027. [PubMed: 26962052]

Owen DR, Yeo AJ, Gunn RN, Song K, Wadsworth G, Lewis A, Rhodes C, Pulford DJ, Bennacef I, Parker CA, StJean PL, Cardon LR, Mooser VE, Matthews PM, Rabiner EA, Rubio JP, 2012. An 18-kDa translocator protein (TSPO) polymorphism explains differences in binding affinity of the PET radioligand PBR28. J. Cereb. Blood Flow Metab 32, 1–5. doi:10.1038/jcbfm.2011.147. [PubMed: 22008728]

Parbo P, Ismail R, Sommerauer M, Stokholm MG, Hansen AK, Hansen KV, Amidi A, Schaldemose JL, Gottrup H, Brændgaard H, Eskildsen SF, Borghammer P, Hinz R, Aanerud J, Brooks DJ, 2018. Does inflammation precede tau aggregation in early Alzheimer's disease? A PET study. Neurobiol. Dis 117, 211–216. doi:10.1016/j.nbd.2018.06.004. [PubMed: 29902557]

Plascencia-Villa G, Ponce A, Collingwood JF, Arellano-Jiménez MJ, Zhu X, Rogers JT, Betancourt I, José-Yacamán M, Perry G, 2016. High-resolution analytical imaging and electron holography of magnetite particles in amyloid cores of Alzheimer's disease. Sci. Rep 6, 24873. doi:10.1038/srep24873. [PubMed: 27121137]

Popescu BFG, Pirko I, Lucchinetti CF, 2013. Pathology of multiple sclerosis: where do we stand? Continuum (Minneap Minn) 19, 901–921. doi:10.1212/01.CON.0000433291.23091.65. [PubMed: 23917093]

Rao IY, Hanson LR, Johnson JC, Rosenbloom MH, Frey WH, 2022. Brain glucose hypometabolism and iron accumulation in different brain regions in Alzheimer's and Parkinson's diseases. Pharmaceuticals (Basel) 15, 551. doi:10.3390/ph15050551. [PubMed: 35631378]

Ravanfar P, Loi SM, Syeda WT, Van Rheenen TE, Bush AI, Desmond P, Cropley VL, Lane DJR, Opazo CM, Moffat BA, Velakoulis D, Pantelis C, 2021. Systematic review: quantitative susceptibility mapping (QSM) of brain iron profile in neurodegenerative diseases. Front. Neurosci 15.

Rotta J, Perosa V, Yakupov R, Kuijf HJ, Schreiber F, Dobisch L, Oltmer J, Assmann A, Speck O, Heinze H-J, Acosta-Cabronero J, Duzel E, Schreiber S, 2021. Detection of cerebral microbleeds with venous connection at 7-Tesla MRI. Neurology 96, e2048–e2057. doi:10.1212/WNL.0000000000011790. [PubMed: 33653897]

Author Manuscript Author Manuscript Author Manuscript Author Manuscript

Satoh R, Arani A, Schwarz C, Senjem M, Ali F, Jack CR Jr, Lowe V, Josephs KA, Whitwell JL, 2023. Subcortical flortaucipir PET and susceptibility analyses to differentiate progressive supranuclear palsy clinical variants and corticobasal syndrome. Human Amyloid Imaging 2023. Presented at the Human Amyloid Imaging 2023.

Schindler SE, Bollinger JG, Ovod V, Mawuenyega KG, Li Y, Gordon BA, Holtzman DM, Morris JC, Benzinger TLS, Xiong C, Fagan AM, Bateman RJ, High-precision plasma β-amyloid 42/40 predicts current and future brain amyloidosis. Neurology 93, e1647–e1659. doi:10.1212/WNL.0000000000008081.

Schweitzer AD, Liu T, Gupta A, Zheng K, Seedial S, Shtilbans A, Shahbazi M, Lange D, Wang Y, Tsiouris AJ, 2015. Quantitative susceptibility mapping of the motor cortex in amyotrophic lateral sclerosis and primary lateral sclerosis. Am. J. Roentgenol 204, 1086–1092. doi:10.2214/AJR.14.13459. [PubMed: 25905946]

Schweser F, Robinson SD, de Rochefort L, Li W, Bredies K, 2017. An illustrated comparison of processing methods for phase MRI and QSM: removal of background field contributions from sources outside the region of interest. NMR Biomed. 30. doi:10.1002/nbm.3604.

Shaw LM, Arias J, Blennow K, Galasko D, Molinuevo JL, Salloway S, Schindler S, Carrillo MC, Hendrix JA, Ross A, Illes J, Ramus C, Fifer S, 2018. Appropriate use criteria for lumbar puncture and cerebrospinal fluid testing in the diagnosis of Alzheimer's disease. Alzheimers Dement. 14, 1505–1521. doi:10.1016/j.jalz.2018.07.220. [PubMed: 30316776]

Shin H-G, Lee Jingu, Yun YH, Yoo SH, Jang J, Oh S-H, Nam Y, Jung S, Kim S, Fukunaga M, Kim W, Choi HJ, Lee Jongho, 2021. χ-separation: magnetic susceptibility source separation toward iron and myelin mapping in the brain. Neuroimage 240, 118371. doi:10.1016/j.neuroimage.2021.118371. [PubMed: 34242783]

Shmueli K, de Zwart JA, van Gelderen P, Li T-Q, Dodd SJ, Duyn JH, 2009. Magnetic susceptibility mapping of brain tissue in vivo using MRI phase data. Magn. Reson. Med 62, 1510–1522. doi:10.1002/mrm.22135. [PubMed: 19859937]

Sjöström H, Granberg T, Westman E, Svenningsson P, 2017. Quantitative susceptibility mapping differentiates between Parkinsonian disorders. Parkinsonism Relat. Disord 44, 51–57. doi:10.1016/j.parkreldis.2017.08.029. [PubMed: 28886909]

Smith MA, Harris PLR, Sayre LM, Perry G, 1997. Iron accumulation in Alzheimer disease is a source of redox-generated free radicals. Proc. Natl. Acad. Sci. USA 94, 9866–9868. [PubMed: 9275217]

Snow BJ, Tooyama I, McGeer EG, Yamada T, Calne DB, Takahashi H, Kimura H, 1993. Human positron emission tomographic [18F]fluorodopa studies correlate with dopamine cell counts and levels. Ann. Neurol 34, 324–330. doi:10.1002/ana.410340304. [PubMed: 8363349]

Sofic E, Riederer P, Heinsen H, Beckmann H, Reynolds GP, Hebenstreit G, Youdim MB, 1988. Increased iron (III) and total iron content in post mortem substantia nigra of Parkinsonian brain. J. Neural. Transm 74, 199–205. doi:10.1007/BF01244786. [PubMed: 3210014]

Sood S, Urriola J, Reutens D, O'Brien K, Bollmann S, Barth M, Vegh V, 2017. Echo time-dependent quantitative susceptibility mapping contains information on tissue properties. Magn. Reson. Med 77, 1946–1958. doi:10.1002/mrm.26281. [PubMed: 27221590]

Spotorno N, Acosta-Cabronero J, Stomrud E, Lampinen B, Strandberg OT, van Westen D, Hansson O, 2020. Relationship between cortical iron and tau aggregation in Alzheimer's disease. Brain 143, 1341–1349. doi:10.1093/brain/awaa089. [PubMed: 32330946]

Stankeviciute L, Falcon C, Operto G, Rojas S, Grau-Rivera O, Garcia M, Shekari M, Niñerola-Baizán A, Perissinotti A, Minguillón C, Fauria K, Molinuevo JL, Zetterberg H, Blennow K, Suárez-Calvet M, Cacciaglia R, Gispert JD, 2022. Associations between brain iron deposition and structural Alzheimer's disease signature in cognitively unimpaired adults. Alzheimer's Dement. 18, e066766. doi:10.1002/alz.066766.

Straub S, Schneider TM, Emmerich J, Freitag MT, Ziener CH, Schlemmer H-P, Ladd ME, Laun FB, 2017. Suitable reference tissues for quantitative susceptibility mapping of the brain. Magn. Reson. Med 78, 204–214. doi:10.1002/mrm.26369. [PubMed: 27529579]

Swanson CJ, Zhang Y, Dhadda S, Wang J, Kaplow J, Lai RYK, Lannfelt L, Bradley H, Rabe M, Koyama A, Reyderman L, Berry DA, Berry S, Gordon R, Kramer LD, Cummings JL, 2021. A randomized, double-blind, phase 2b proof-of-concept clinical trial in early Alzheimer's disease

Author Manuscript Author Manuscript Author Manuscript Author Manuscript

with lecanemab, an anti-Aβ protofibril antibody. Alzheimer's Res. Ther 13, 80. doi:10.1186/s13195-021-00813-8. [PubMed: 33865446]

Takada H, Nagata K, Hirata Y, Satoh Y, Watahiki Y, Sugawara J, Yokoyama E, Kondoh Y, Shishido F, Inugami A, 1992. Age-related decline of cerebral oxygen metabolism in normal population detected with positron emission tomography. Neurol. Res 14, 128–131. doi:10.1080/01616412.1992.11740031. [PubMed: 1355868]

Telling ND, Everett J, Collingwood JF, Dobson J, van der Laan G, Gallagher JJ, Wang J, Hitchcock AP, 2017. Iron biochemistry is correlated with amyloid plaque morphology in an established mouse model of Alzheimer's disease. Cell Chem. Biol 24. doi:10.1016/j.chembiol.2017.07.014, 1205–1215.e3. [PubMed: 28890316]

Therriault J, Pascoal TA, Lussier FZ, Tissot C, Chamoun M, Bezgin G, Servaes S, Benedet AL, Ashton NJ, Karikari TK, Lantero-Rodriguez J, Kunach P, Wang Y-T, Fernandez-Arias J, Massarweh G, Vitali P, Soucy J-P, Saha-Chaudhuri P, Blennow K, Zetterberg H, Gauthier S, Rosa-Neto P, 2022. Biomarker modeling of Alzheimer's disease using PET-based Braak staging. Nat. Aging 2, 526–535. doi:10.1038/s43587-022-00204-0. [PubMed: 37118445]

Tiepolt S, Rullmann M, Patt M, Jochimsen T, Karl-Titus H, Schroeter M, Sabri O, Barthel H, 2021. Quantitative susceptibility mapping (QSM) MRI in patients with behavioral-variant frontotemporal dementia (bvFTD) - incremental value to brain PET? J. Nucl. Med 62, 1079.

Tiepolt S, Schäfer A, Rullmann M, Roggenhofer E, Gertz H-J, Schroeter ML, Patt M, Bazin P-L, Jochimsen TH, Turner R, Sabri O, Barthel HNetherlands Brain Bank, 2018. Quantitative susceptibility mapping of amyloid-β aggregates in Alzheimer's disease with 7T MR. J. Alzheimers Dis 64, 393–404. doi:10.3233/JAD-180118. [PubMed: 29865069]

Tohgi H, Yonezawa H, Takahashi S, Sato N, Kato E, Kudo M, Hatano K, Sasaki T, 1998. Cerebral blood flow and oxygen metabolism in senile dementia of Alzheimer's type and vascular dementia with deep white matter changes. Neuroradiology 40, 131–137. doi:10.1007/s002340050553. [PubMed: 9561514]

Tu J, Yan J, Liu J, Liu D, Wang X, Gao F, 2022. Iron deposition in the precuneus is correlated with mild cognitive impairment in patients with cerebral microbleeds: a quantitative susceptibility mapping study. Front. Neurosci 16, 944709. doi:10.3389/fnins.2022.944709. [PubMed: 36003962]

Uchida Y, Kan H, Sakurai K, Oishi K, Matsukawa N, 2022. Quantitative susceptibility mapping as an imaging biomarker for Alzheimer's disease: the expectations and limitations. Front. Neurosci 16, 938092. doi:10.3389/fnins.2022.938092. [PubMed: 35992906]

van Bergen JMG, Li X, Quevenco FC, Gietl AF, Treyer V, Meyer R, Buck A, Kaufmann PA, Nitsch RM, van Zijl PCM, Hock C, Unschuld PG, 2018. Simultaneous quantitative susceptibility mapping and Flutemetamol-PET suggests local correlation of iron and β-amyloid as an indicator of cognitive performance at high age. Neuroimage 174, 308–316. doi:10.1016/j.neuroimage.2018.03.021. [PubMed: 29548847]

Vemuri P, Decarli C, Duering M, 2022. Imaging markers of vascular brain health: quantification, clinical implications, and future directions. Stroke 53, 416–426. doi:10.1161/STROKEAHA.120.032611. [PubMed: 35000423]

Vinayagamani S, Sheelakumari R, Sabarish S, Senthilvelan S, Ros R, Thomas B, Kesavadas C, 2021. Quantitative susceptibility mapping: technical considerations and clinical applications in neuroimaging. J. Magn. Reson. Imaging 53, 23–37. doi:10.1002/jmri.27058. [PubMed: 31951057]

Vogel JW, Young AL, Oxtoby NP, Smith R, Ossenkoppele R, Strandberg OT, La Joie R, Aksman LM, Grothe MJ, Iturria-Medina Y, Pontecorvo MJ, Devous MD, Rabinovici GD, Alexander DC, Lyoo CH, Evans AC, Hansson OAlzheimer's Disease Neuroimaging Initiative, 2021. Four distinct trajectories of tau deposition identified in Alzheimer's disease. Nat. Med 27, 871–881. doi:10.1038/s41591-021-01309-6. [PubMed: 33927414]

Wang Y, Liu T, 2015. Quantitative susceptibility mapping (QSM): decoding MRI data for a tissue magnetic biomarker. Magn. Reson. Med 73, 82–101. doi:10.1002/mrm.25358. [PubMed: 25044035]

Wang Y, Spincemaille P, Liu Z, Dimov A, Deh K, Li J, Zhang Y, Yao Y, Gillen KM, Wilman AH, Gupta A, Tsiouris AJ, Kovanlikaya I, Chiang GC-Y, Weinsaft JW, Tanenbaum L, Chen W,

Author Manuscript Author Manuscript Author Manuscript Author Manuscript

Zhu W, Chang S, Lou M, Kopell BH, Kaplitt MG, Devos D, Hirai T, Huang X, Korogi Y, Shtilbans A, Jahng G-H, Pelletier D, Gauthier SA, Pitt D, Bush AI, Brittenham GM, Prince MR, 2017. Clinical quantitative susceptibility mapping (QSM): biometal imaging and its emerging roles in patient care. J. Magn. Reson. Imaging 46, 951–971. doi:10.1002/jmri.25693. [PubMed: 28295954]

Whitwell JL, Lowe VJ, Tosakulwong N, Weigand SD, Senjem ML, Schwarz C, Spychalla AJ, Petersen RC, Jack CR, Josephs KA, 2017. [18F]AV1451 tau-PET in progressive supranuclear palsy. Mov. Disord 32, 124–133. doi:10.1002/mds.26834. [PubMed: 27787958]

Yamaguchi T, Kanno I, Uemura K, Shishido F, Inugami A, Ogawa T, Murakami M, Suzuki K, 1986. Reduction in regional cerebral metabolic rate of oxygen during human aging. Stroke 17, 1220–1228. doi:10.1161/01.str.17.6.1220. [PubMed: 3492786]

Yamaji S, Ishii K, Sasaki M, Imamura T, Kitagaki H, Sakamoto S, Mori E, 1997. Changes in cerebral blood flow and oxygen metabolism related to magnetic resonance imaging white matter hyperintensities in Alzheimer's disease. J. Nucl. Med 38, 1471–1474. [PubMed: 9293811]

Yang Z, Zan Y, Zheng X, Hai W, Chen K, Huang Q, Xu Y, Peng J, 2015. Dynamic FDG-PET imaging to differentiate malignancies from inflammation in subcutaneous and in situ mouse model for non-small cell lung carcinoma (NSCLC). PLoS One 10, e0139089. doi:10.1371/journal.pone.0139089. [PubMed: 26421925]

Zanotti-Fregonara P, Pascual B, Veronese M, Yu M, Beers D, Appel SH, Masdeu JC, 2019. Head-to-head comparison of 11C-PBR28 and 11C-ER176 for quantification of the translocator protein in the human brain. Eur. J. Nucl. Med. Mol. Imaging 46, 1822–1829. doi:10.1007/s00259-019-04349-w. [PubMed: 31152207]

Zeineh MM, Chen Y, Kitzler HH, Hammond R, Vogel H, Rutt BK, 2015. Activated iron-containing microglia in the human hippocampus identified by magnetic resonance imaging in Alzheimer disease. Neurobiol. Aging 36, 2483–2500. doi:10.1016/j.neurobiolaging.2015.05.022. [PubMed: 26190634]

Zhao P, Zhang B, Gao S, Li X, 2020. Clinical features, MRI, and 18F-FDG-PET in differential diagnosis of Parkinson disease from multiple system atrophy. Brain Behav. 10, e01827. doi:10.1002/brb3.1827. [PubMed: 32940411]

Zimmer ER, Parent MJ, Souza DG, Leuzy A, Lecrux C, Kim H-I, Gauthier S, Pellerin L, Hamel E, Rosa-Neto P, 2017. [18F]FDG PET signal is driven by astroglial glutamate transport. Nat. Neurosci 20, 393–395. doi:10.1038/nn.4492. [PubMed: 28135241]

Author Manuscript Author Manuscript Author Manuscript Author Manuscript

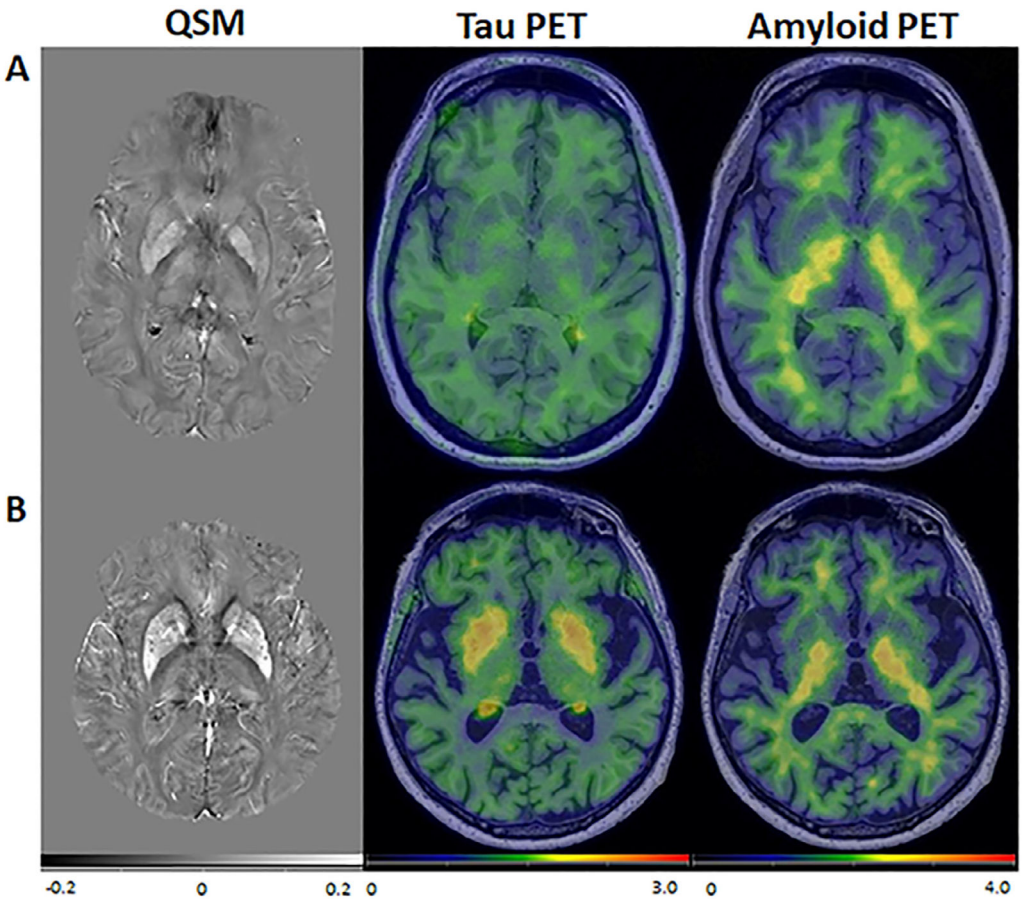

Fig. 1.

QSM, tau PET and amyloid PET in two representative participants. (A) a 35-year-old participant and (B) and 83-year-old participant, both cognitively unimpaired. In the older participant, there was elevated susceptibility and tau PET SUVR in the basal ganglia. Amyloid PET SUVR was low throughout for both participants. Figure reproduced from Cogswell et al., NeuroImage 2021.

Author Manuscript Author Manuscript Author Manuscript Author Manuscript

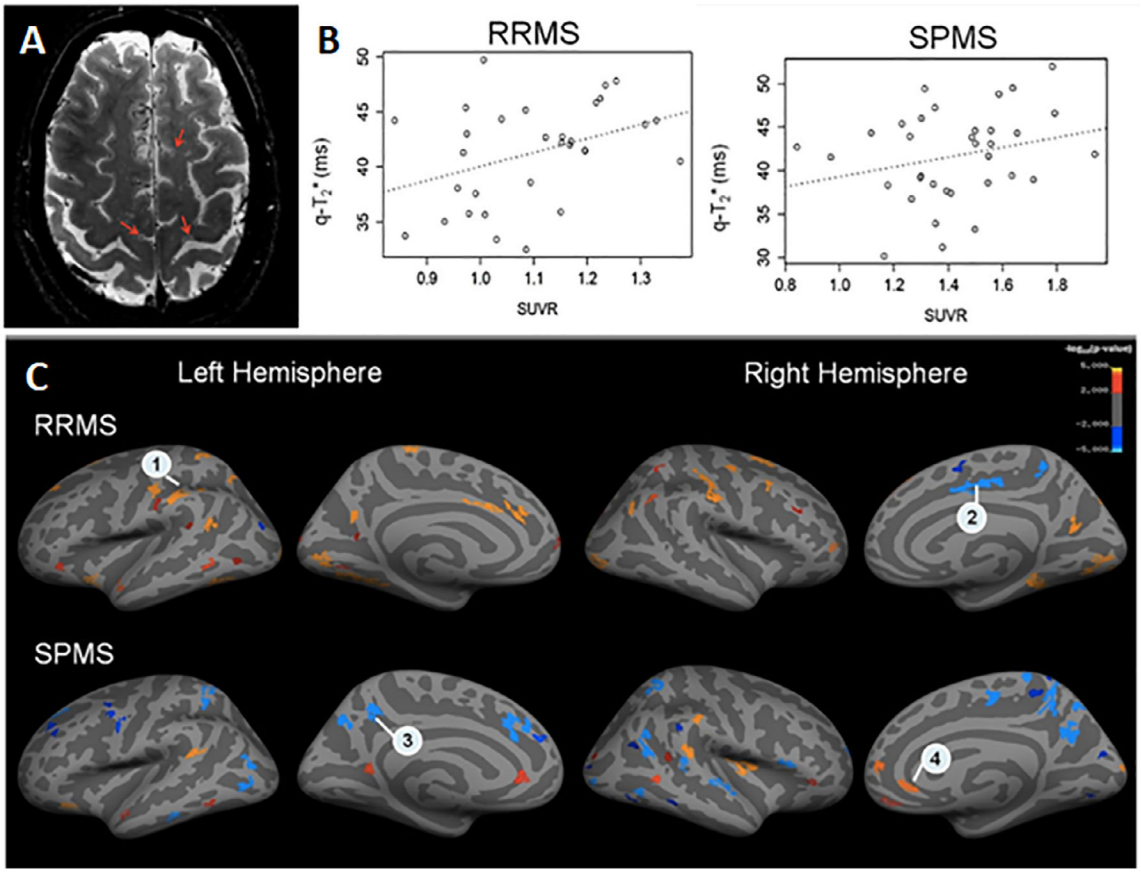

Fig. 2.

(A) Axial 7 Tesla T2*-weighted image with example cortical lesions in a 59-year-old patient with SPMS. (B) Correlation between TSPO-PET standardized uptake value (SUVR) and T2* signal across individual cortical lesions in a 48-year-old patient with RR MS (left) and a 40-year-old patient with SPMS (right), $p < 0.05$. (C) Areas of correlation between T2* -signal at 7 Tesla and TSPO-PET signal sampled along the cortical surface, averaged across patients in each MS group. RRMS = relapsing remitting multiple sclerosis; SPMS = secondary progressive multiple sclerosis. Reproduced with permission from Herranz et al., Mult Scler 2020.

Author Manuscript Author Manuscript Author Manuscript Author Manuscript

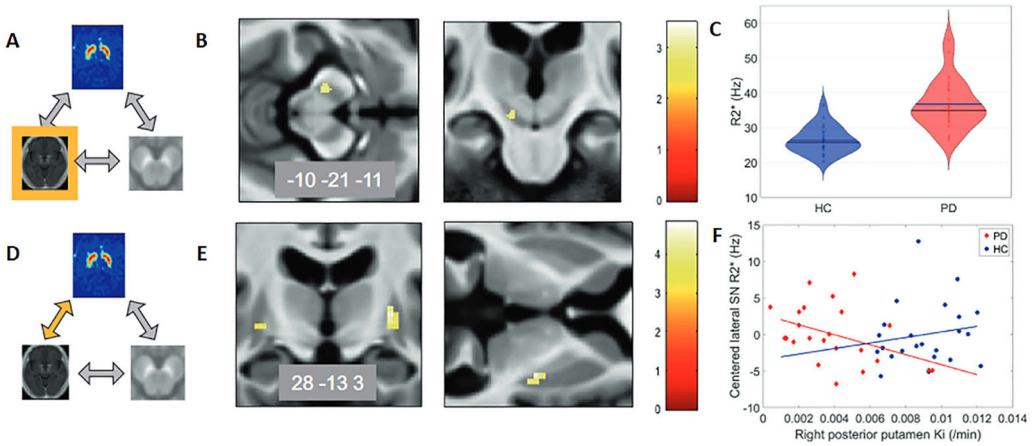

Fig. 3.

Relationships between 18F-DOPA PET and R2* in Parkinson's disease. Depierreux et al. studied the relationships between 18F-DOPA PET, R2* MRI, and neuromelanin-sensitive MRI. The figure has been adapted to demonstrate the relationships between 18F-DOPA PET and R2* MRI. (A–C) R2* changes in Parkinson's disease (PD). (A) Schematic of modality or association being studied, which is highlighted in yellow, in this case R2* MRI. (B) Color map (*t*-values) of disease effects on brain iron as assessed by R2* , $p < 0.001$, overlaid on the mean T1-weighted image of the population. Unilateral increase in substantia nigra (SN) R2* in PD. (C) Violin plot of substantia nigra R2* in PD compared to healthy controls (HC). (D-F) Relationship between 18F-DOPA PET and R* MRI, indicated by the yellow arrow. (E) Color map of regions on 18F-DOPA PET that showed a different relationship with (SN) R2* in PD vs. HC. (F) In PD, SN R2* decreased with higher 18F-DOPA PET Ki ($p = 0.024$) vs. increase in HC. Figure adapted from Depierreux et al., NPJ Parkinson's Disease 2021.

Author Manuscript Author Manuscript Author Manuscript Author Manuscript

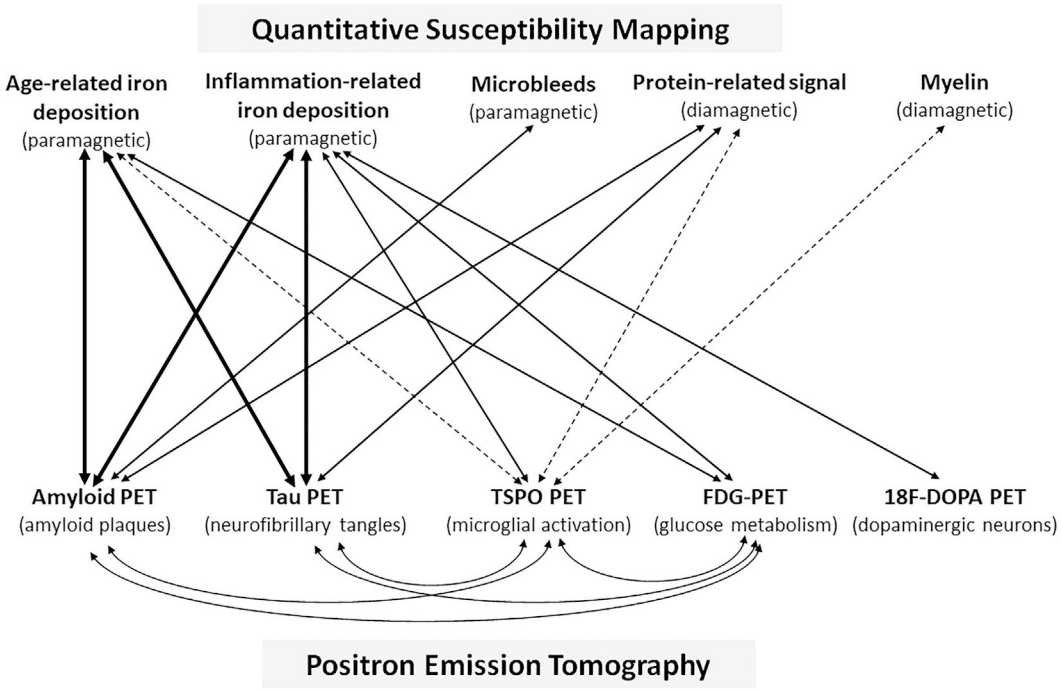

Fig. 4.

Schematic QSM-PET associations. Sources of QSM signal and their relative diamagnetic or paramagnetic susceptibility are listed on the top. PET tracers and their target are listed on the bottom. Solid lines indicate relationships that have been identified in prior work, and the width of the line indicates, qualitatively, the relative strength of those associations. Proposed relationships, which have yet to be studied are indicated by dashed lines.